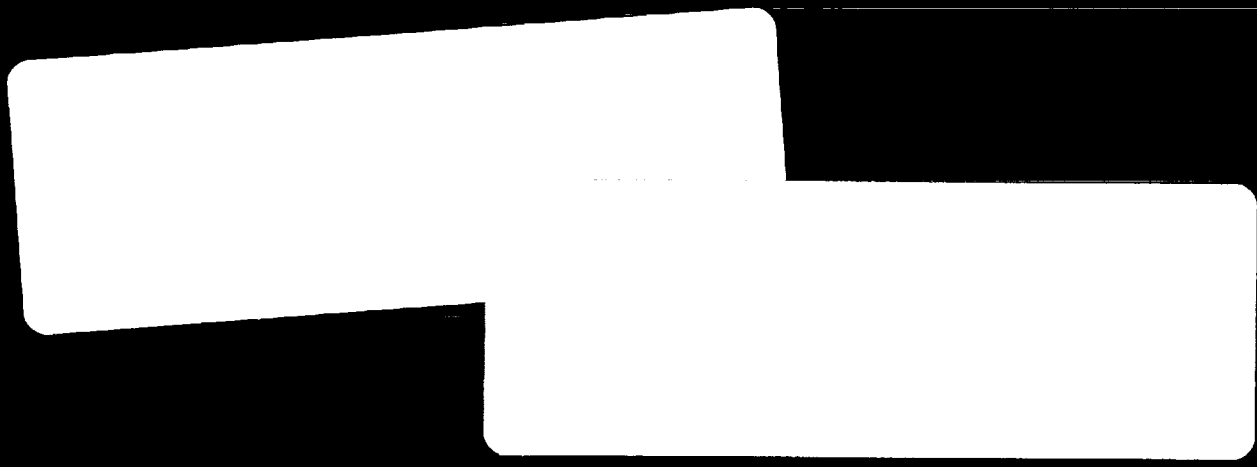

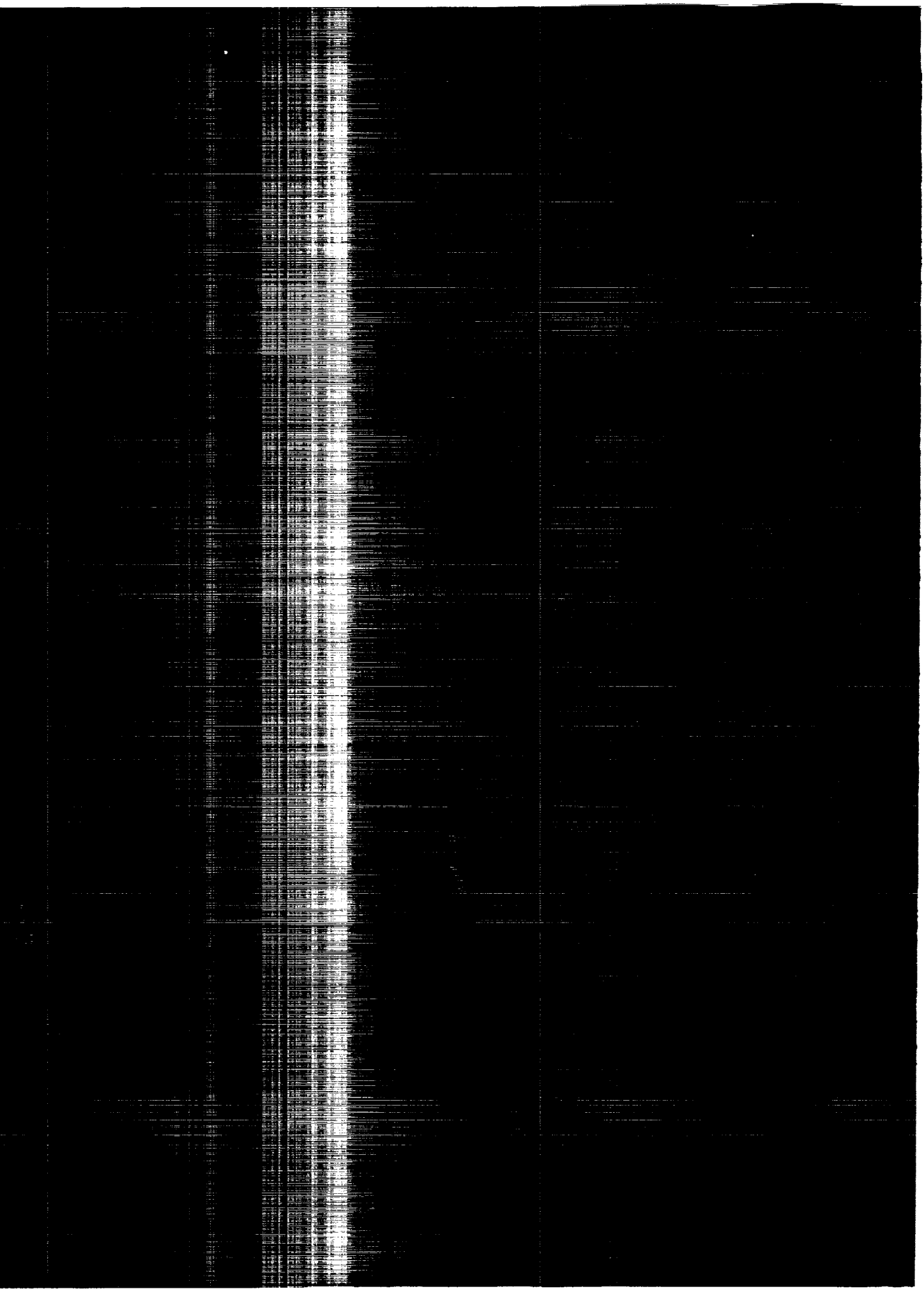

[redacted]

[redacted]

1. Report No. NASA TM X-2571	2. Government Accession No.	3. Recipient's Catalog No.
4. Title and Subtitle LOW-SPEED AERODYNAMIC CHARACTERISTICS OF A 17-PERCENT-THICK SUPERCRITICAL AIRFOIL SECTION, INCLUDING A COMPARISON BETWEEN WIND-TUNNEL AND FLIGHT DATA (U)		5. Report Date July 1972 6. Performing Organization Code
7. Author(s) Robert J. McGhee; and Gene J. Bingham (Langley Directorate, U.S. Army Air Mobility R & D Laboratory)		8. Performing Organization Report No. L-8290 10. Work Unit No. 742-73-02-03
9. Performing Organization Name and Address NASA Langley Research Center Hampton, Va. 23365		11. Contract or Grant No. 13. Type of Report and Period Covered Technical Memorandum
12. Sponsoring Agency Name and Address National Aeronautics and Space Administration Washington, D.C. 20546		14. Sponsoring Agency Code

15. Supplementary Notes

16. Abstract

Wind-tunnel tests have been conducted to determine the low-speed two-dimensional aerodynamic characteristics of a 17-percent-thick supercritical airfoil. The results were compared with three-dimensional wind-tunnel and flight data. The tests were conducted over a Mach number range from 0.15 to 0.30. Reynolds numbers based on the airfoil chord varied from 2.0×10^6 to 25.0×10^6.

17. Key Words (Suggested by Author(s))

Supercritical airfoil section
Low-speed aerodynamics
High Reynolds numbers

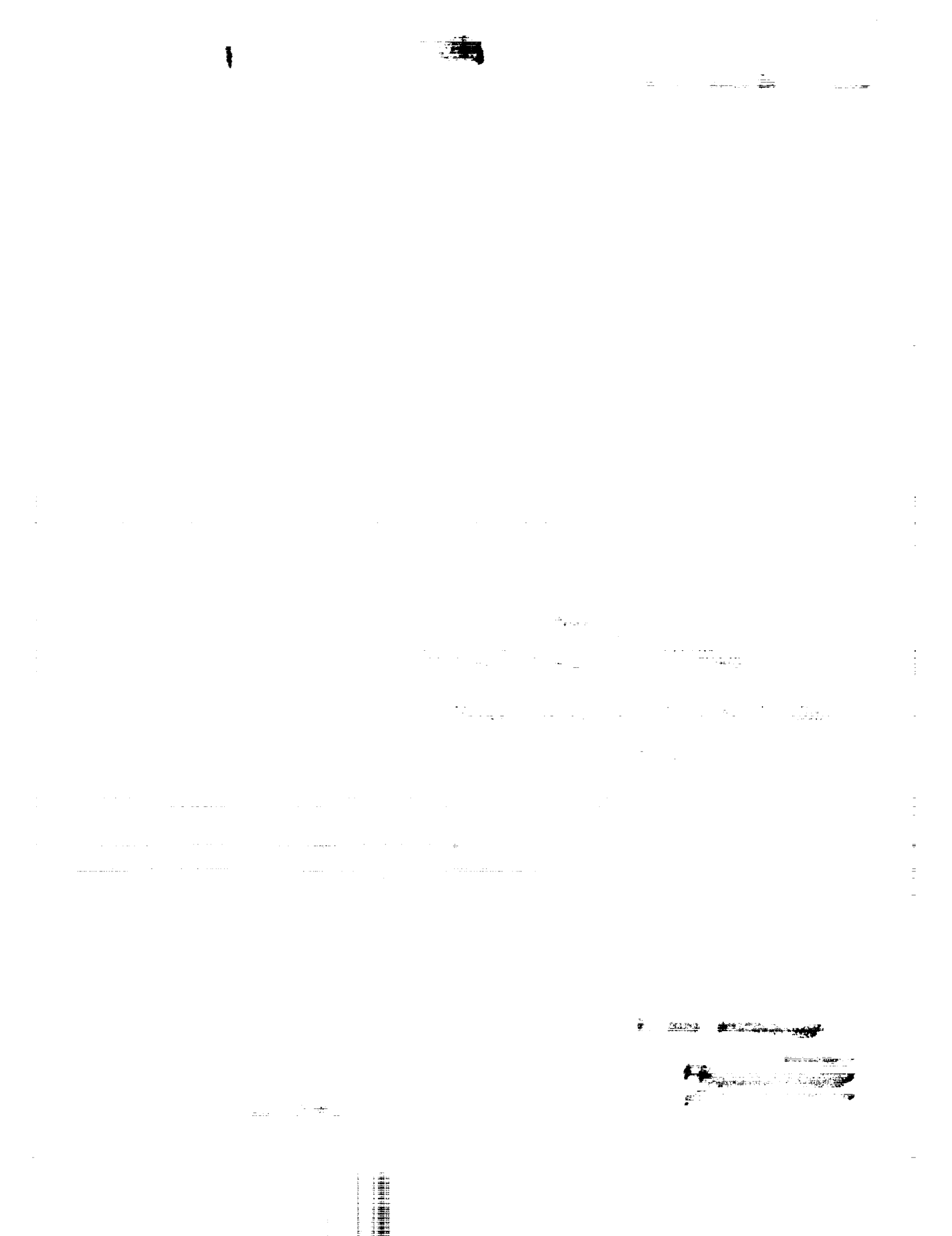

LOW-SPEED AERODYNAMIC CHARACTERISTICS OF A 17-PERCENT-THICK SUPERCRITICAL AIRFOIL SECTION, INCLUDING A COMPARISON BETWEEN WIND-TUNNEL AND FLIGHT DATA*

By Robert J. McGhee
Langley Research Center

and

Gene J. Bingham
Langley Directorate, U.S. Army Air Mobility R & D Laboratory

SUMMARY

An investigation was conducted in the Langley low-turbulence pressure tunnel to determine the low-speed two-dimensional aerodynamic characteristics of a 17-percent-thick supercritical airfoil. The results were compared with three-dimensional wind-tunnel and flight data. The tests were conducted over a Mach number range from 0.15 to 0.30. Reynolds numbers, based on the airfoil chord, were varied from 2.0×10^6 to 25.0×10^6.

The results of the investigation indicate that maximum section lift coefficients greater than 2.0 were obtained at test Reynolds numbers above 5.0×10^6. Maximum section lift coefficients increased rapidly at Reynolds numbers from 2.0×10^6 to 5.0×10^6. A measurable decrease in maximum section lift coefficient occurred at a Mach number of 0.15 as the Reynolds number was increased from about 9.0×10^6 to 17.0×10^6. A decrease in maximum section lift coefficient of about 10 percent occurred when the Mach number was increased from 0.22 to 0.30, and the stall became less abrupt; these effects are a result of the flow over the airfoil becoming supercritical. The lift-curve slopes of the corrected two-dimensional data were in good agreement with the lift-curve slopes obtained from three-dimensional wind-tunnel and flight data.

INTRODUCTION

Research on supercritical airfoils conducted at Langley Research Center over the last several years has been directed toward improving performance by increasing the drag-divergence Mach number. Thus, the cruising speeds of aircraft that employ wings

---

*Title, Unclassified.

with supercritical airfoil sections may be substantially increased. The improved performance is accomplished by delaying the onset of shock-induced flow separation over the airfoil and is accompanied by delayed buffet onset of the wing. Wind-tunnel investigations of supercritical airfoils are reported in references 1 and 2.

These new airfoils have applications to subsonic transports and other long-range airplanes. This concept can be applied to increasing the wing thickness of airfoils without the reduction in drag-divergence Mach number that is normally incurred with increase in the thickness ratio of conventional airfoils. As a result, the advantages of more volume for fuel or for blown high-lift devices, increased aspect ratio, and lower structural weight may be achieved with the use of high-thickness-ratio supercritical airfoil sections. Reference 3 presents both wind-tunnel and flight results on a 17-percent-thick supercritical airfoil employed on a T-2C airplane. The results in reference 3 show definite performance gains for the 17-percent-thick supercritical airfoil compared with the basic NACA 64A212 airfoil originally employed on the T-2C airplane.

The present investigation was conducted to determine the basic low-speed two-dimensional aerodynamic characteristics of the 17-percent-thick supercritical airfoil of reference 3 and to provide information on the effects of Reynolds number. In addition, the results were to be compared with other wind-tunnel results and flight data. The investigation was performed in the Langley low-turbulence pressure tunnel over a Mach number range from 0.15 to 0.30. The Reynolds number, based on airfoil chord, varied from 2.0×10^6 to 25.0×10^6. The geometrical angle of attack varied from about -10^o to 24^o.

SYMBOLS

Values are given both in the SI and the U.S. Customary Units. The measurements and calculations were made in the U.S. Customary Units.

C_p pressure coefficient, $\frac{p_L - p_\infty}{q_\infty}$

c chord of airfoil, cm (in.)

c_c section chord-force coefficient, $\int_{\substack{\text{forward} \\ (t/c)_{max}}} C_p \, d\left(\frac{z}{c}\right) - \int_{\substack{\text{aft} \\ (t/c)_{max}}} C_p \, d\left(\frac{z}{c}\right)$

c_d section pressure-drag coefficient, $c_n \sin \alpha + c_c \cos \alpha$

$c_{d,w}$ section profile-drag coefficient determined from wake measurements, $\int_{wake} c_d' \, d\left(\frac{h}{c}\right)$

c_d' point drag coefficient, $2\left(\frac{\rho_1}{\rho_2}\right)^{1/2}\left(\frac{q_1}{q_\infty}\right)^{1/2}\left[\left(\frac{\rho_2}{\rho_\infty}\right)^{1/2} - \left(\frac{q_2}{q_\infty}\right)^{1/2}\right]$

c_l section lift coefficient, $c_n \cos \alpha - c_c \sin \alpha$

c_m section pitching-moment coefficient about quarter chord, $\int_{l.s.} C_p \, d\left(\frac{x}{c}\right)\left(0.25 - \frac{x}{c}\right) - \int_{u.s.} C_p \, d\left(\frac{x}{c}\right)\left(0.25 - \frac{x}{c}\right)$

c_n section normal-force coefficient, $\int_{l.s.} C_p \, d\left(\frac{x}{c}\right) - \int_{u.s.} C_p \, d\left(\frac{x}{c}\right)$

h vertical distance in wake profile, cm (in.)

l/d section lift-drag ratio, $c_l/c_{d,w}$

M free-stream Mach number

p static pressure, N/m^2 (lb/ft^2)

q dynamic pressure, N/m^2 (lb/ft^2)

R Reynolds number based on free-stream conditions and airfoil chord

t airfoil thickness, cm (in.)

x airfoil abscissa, cm (in.)

y spanwise distance from airfoil plane of symmetry, cm (in.)

z airfoil ordinate, cm (in.)

α angle of attack of airfoil, angle between chord line and airstream axis, deg

α_{ref} angle of attack of wing planform at root chord, deg

ρ density, kg/m^3 ($slugs/ft^3$)

Subscripts:

c	mean camber line
cr	critical (refers to local Mach number of 1)
L	local point on airfoil
max	maximum
∞	undisturbed stream conditions
1	tunnel station 1 chord length downstream of model
2	tunnel station downstream of model where density is equal to free-stream density

ABBREVIATIONS

l.s.	lower surface
u.s.	upper surface
TPT	transonic pressure tunnel
LTPT	low-turbulence pressure tunnel
2-D	two-dimensional
3-D	three-dimensional

APPARATUS AND PROCEDURES

Airfoil Design

The design procedures used in obtaining the supercritical airfoil shape are given in detail in reference 3. At design conditions the airfoil is shaped to produce supersonic expansion waves over the airfoil upper surface which are reflected from the sonic boundary as compression waves. The reflected compression waves result in a more nearly isentropic recompression; the strength of the shock wave and the tendency toward

shock-induced flow separation are thereby reduced. The resulting airfoil has a relatively flat upper and lower surface and a large leading-edge radius. Figure 1 illustrates the airfoil section shape and table I presents the airfoil coordinates. Figure 2 presents the camber line for the airfoil. Additional discussions of the design concepts and early design philosophy of supercritical airfoils are reported in references 1 and 2.

Wind Tunnel

The Langley low-turbulence pressure tunnel (ref. 4) is a closed-throat single-return tunnel which can be operated at stagnation pressures from 101.3 to 1013 kN/m^2 (1 to 10 atm) with tunnel-empty test-section Mach numbers up to 0.46 and 0.23, respectively. The maximum unit Reynolds number is about 49×10^6 per meter (15×10^6 per foot) at a Mach number of 0.23. The test section is 91.44 cm (3 ft) wide by 228.6 cm (7.5 ft) high. The two-dimensional airfoil was attached through a two-component force balance at each end to circular end plates, 101.6 cm (40 in.) in diameter, which are flush with the tunnel wall and are hydraulically actuated to provide for model angle of attack. (See fig. 3.) Since the balances were new and uncalibrated, they were used only as model supports for this test. The air gap between the balance adaptor plates and airfoil was sealed. The model was mounted with the quarter chord coincident with the rotational axis of the circular plates.

Model

The airfoil model was machined from a solid aluminum billet and had a chord of 58.42 cm (23 in.) and a span of 91.44 cm (3 ft) to span the wind tunnel completely. Figure 4 shows a photograph of the airfoil mounted in the wind tunnel. The model was equipped with both upper-surface and lower-surface orifices which were drilled perpendicular to the local surface of the airfoil with a drill diameter of 0.08128 cm (0.032 in.) and were located at the chord stations indicated in table II. Spanwise pressure orifices were also located on the airfoil upper surface at $\frac{x}{c} = 0.70$ as indicated in figure 3. In addition, a base pressure orifice was included in the blunt trailing edge of the airfoil.

Wake Survey Rake

A fixed wake survey rake (fig. 5) was mounted on the tunnel side wall and located 1 chord length rearward of the trailing edge of the airfoil. The wake rake utilized 91 total-pressure tubes and five static-pressure tubes 0.1524 cm (0.060 in.) in diameter. The total-pressure tubes were flattened to 0.1016 cm (0.040 in.). The static tubes had four flush orifices drilled 90° apart and located 8 tube diameters from the tip of the tube and in the plane of the total-pressure tubes.

Instrumentation

Measurements of the static pressures on the airfoil surface and the wake-rake pressures were made by an automatic pressure-scanning system and were recorded on punched cards. Basic tunnel pressures (stagnation pressure and stagnation pressure minus reference static pressure) were measured with precision quartz pressure meters and recorded on punched cards. Angle of attack was measured with a calibrated potentiometer attached to the circular plates.

TEST AND METHODS

The airfoil was investigated at Mach numbers from 0.15 to 0.30. Reynolds number based on the airfoil chord was varied from 2.0×10^6 to 25.0×10^6, primarily by varying the tunnel stagnation pressure. The geometric angle of attack varied from about -10° to 24°. The airfoil was tested smooth (natural boundary-layer transition); however, for several test conditions boundary-layer transition strips, sized according to reference 5, were located on both the upper and lower surfaces of the model. The strips were 0.25 cm (0.10 in.) wide and set in a plastic adhesive. The grit was sparsely spaced and attached to the surface with lacquer. For several test runs, oil was spread over the airfoil upper surface to determine the local flow streamline patterns.

The static-pressure measurements at the airfoil surface were reduced to standard pressure coefficients and then machine integrated to obtain section normal-force and chord-force coefficients and section pitching-moment coefficients about the quarter chord.

Section profile-drag coefficient was computed from the wake-rake measurements by the method of reference 6. The profiles showed considerable scatter which is reflected in the plots of $c_{d,w}$. One probable explanation for this scatter may be the unsteady pressures in the wake of the airfoil associated with the wake region behind an airfoil with a blunt base. For this reason, both the profile drag and the pressure drag are included. The pressure drag was obtained from surface-pressure integrations and does not include the skin-friction drag.

An estimate of the standard low-speed wind-tunnel boundary corrections as calculated by the method of reference 7 indicated that these corrections (less than 2 percent) are within the accuracy of the data and have not been applied.

RESULTS

The results of this investigation have been reduced to coefficient form and are presented in the following figures:

DISCUSSION

Wind-Tunnel Results

Pressure distributions.- The spanwise pressure distributions (fig. 6) obtained at $x/c = 0.70$ show only small variations in static pressure across the airfoil span as long as little or no flow separation exists. Thus, two-dimensional flow is indicated.

The chordwise pressure data of figure 7 for the Mach number range tested and $R \approx 9.0 \times 10^6$ show a continual increase in the peak negative values of C_p up to the angle of attack of maximum lift. Upper- and lower-surface pressure coefficients equal to approximately zero or slightly positive values are indicated at the airfoil trailing edge. At the angle of attack of maximum lift, trailing-edge flow separation at about $\frac{x}{c} = 0.85$ is indicated by the region of approximately constant pressure on the upper surface of the airfoil. At airfoil stall, flow separation extends from $\frac{x}{c} = 0.15$ to the trailing edge of the airfoil upper surface and is accompanied by a large decrease in the negative pressure peak. (See fig. 7(b), $\alpha = 19.58^\circ$ and 20.54°.) The scatter of the pressure coefficients at stalled conditions near the leading edge ($\alpha = 20.54^\circ$) may well be related to flow unsteadiness. More pressure recovery near the airfoil leading edge is shown than a laminar boundary layer can withstand without separating; therefore, transition to turbulent flow must have occurred and the airfoil stall is of the turbulent, or trailing-edge, type. (See ref. 8.) Increasing the Mach number from 0.22 to 0.30 resulted in a small region of

supercritical flow over the airfoil at the highest test lift coefficient ($c_l = 1.81$) as indicated by figure 7(c). ($C_{p,sonic}$ for $M = 0.22$ is -13.40, whereas at $M = 0.30$, $C_{p,sonic} = -6.95$.)

At a Reynolds number of 2.0×10^6, figure 8(a) shows a small region of constant pressure near the upper-surface leading edge of the airfoil for angles of attack less than about 3^o. Oil-flow tests showed that a laminar separation bubble was located in this region. Flow reattachment was observed at the downstream edge of the bubble and a turbulent boundary layer followed. Increasing the angle of attack, figure 8(a), from -3^o to 3^o caused the bubble to move progressively forward. Above $\alpha \approx 3^o$, the constant-pressure region is no longer apparent; however, a small bubble probably existed even at higher angles of attack. An angle of attack of 3^o was selected to show the effect of increasing the Reynolds number on this laminar bubble (fig. 8(b)). The bubble is not apparent when the Reynolds number is increased to 5.5×10^6; only a minor irregularity in the pressure gradient is shown just rearward of the maximum negative pressure following a pressure recovery of about 10 percent. Reference 9 presents both pressure data and boundary-layer measurements on an airfoil where similar laminar flow separation with turbulent reattachment was present.

Figures 9(a) and 9(b) show the expected increase in pressure recovery on the rear of the airfoil upper surface at small and moderate angles of attack as the Reynolds number is increased. Figure 9(c) shows that increasing the Reynolds number from 2.0×10^6 to 17×10^6 near the angle of attack for maximum lift resulted in more pressure recovery on the airfoil upper surface and that the region of turbulent separation near the trailing edge is about the same extent at both angles of attack. The airfoil section lift increases to a higher angle of attack before stall than is possible at the lower Reynolds numbers. The pressure data of figures 9(d) and 9(e) indicate a small increase in upper-surface trailing-edge flow separation at the higher angles of attack as the Reynolds number is increased from about 9.0×10^6 to 17.0×10^6. This increase in separation amounts to about 0.05c at a Mach number of 0.15 and a lift coefficient of about 2.0. Additional discussions of the occurrence of this phenomenon on other airfoils may be found in references 9, 10, and 11. The increase in trailing-edge separation at the higher test Reynolds number results in a decrease in maximum lift and is discussed in the following section.

Lift.- A lift-curve slope of about 0.12 per degree and a lift coefficient of about 0.40 at $\alpha = 0^o$ was obtained at all Mach numbers and Reynolds numbers of the investigation (fig. 10). Maximum section lift coefficient increased from about 1.67 to 2.14 as the Reynolds number was increased from 2.0×10^6 to 9.3×10^6 at $M = 0.15$ (figs. 10(a) and 12), with the most rapid increase occurring between Reynolds numbers of 2.0×10^6 and 5.5×10^6. Increasing the Reynolds number to 17×10^6 resulted in a decrease in the lift-curve slope at high angles of attack and a decrease in $(c_l)_{max}$ from about 2.14 to

2.04. Reference 10 suggests that increasing Reynolds number may have either a favorable or unfavorable effect on $(c_l)_{max}$, especially when local laminar separation is present. The favorable effect can result in thinning of the boundary layer as the Reynolds number is increased. The unfavorable influence can result from a change in the flow reattachment location of the laminar bubble with increasing Reynolds number. In the latter case, the initial thickness of the reattached turbulent boundary layer may be altered from that at the lower Reynolds numbers to result in a forward movement of the trailing-edge separation point. It appears that the favorable influence of Reynolds number was realized up to $R = 9.3\times10^6$ and an unfavorable effect became dominant at $R = 17.0\times10^6$. The pressure data, as previously discussed, are consistent with this conclusion because trailing-edge separation moved forward along the airfoil at the higher Reynolds number (figs. 9(d) and 9(e)). This forward movement of separation also occurred at $M = 0.22$, but was not as pronounced and did not result in a measurable loss in lift coefficient. Similar results were observed for an NACA 8318 airfoil (ref. 11) and in unpublished data (obtained in the Langley low-turbulence pressure tunnel) for an NACA 6716 airfoil (fig. 12). Figure 12 also indicates that $(c_l)_{max}$ for the 17-percent-thick supercritical airfoil is about the same as for the NACA 6716 airfoil. The effect of Reynolds number on $(c_l)_{max}$ for several other NACA airfoils is also shown in figure 12 (from ref. 14).

The section lift coefficients at $M = 0.15$ and 0.22 decreased abruptly at stall (figs. 10(a) and 10(b)). The flight-test results of reference 3 also indicated the stall at $M = 0.15$ to be abrupt. However, at a Mach number of 0.30 (fig. 10(c)), the lift curve was rounded, the stall was less severe, and the angle of attack for maximum lift decreased about 5°. A decrease in maximum lift from about 2.04 ($M = 0.22$) to about 1.80 ($M = 0.30$) was measured for $R \approx 9.0 \times 10^6$. This decrease in $(c_l)_{max}$ and change in type of stall is associated with the flow over the airfoil becoming supercritical, as indicated by figures 10 and 13. (M_{cr} was based on the measured pressures and calculated by using the method of ref. 12.)

The addition of artificial boundary-layer-transition strips (fig. 11(a)) had only small effects on the lift data up to and including stall. Figure 8(a) shows that the leading-edge laminar bubble was located near the 0.05c station (the most forward roughness location) at $R = 2 \times 10^6$. Therefore, for this airfoil, boundary-layer transition occurred at or ahead of the most forward transition-strip location on the airfoil upper surface. Because of the favorable pressure gradients on the lower surface at nearly all positive angles of attack, the grit may not have caused transition to occur at all under these conditions.

Pitching moment.- The pitching-moment-coefficient data (fig. 10) were generally insensitive to Reynolds number up to airfoil stall. The data show a change in the slope of c_m versus α from negative to slightly positive for angles of attack greater than

about 4°. A rapid forward movement in center of pressure with increasing α is also indicated by the essentially constant values of c_m and increasing values of c_l. Note that negative values of c_m resulting from the aft loading of the airfoil occur throughout the angle-of-attack range. Employing boundary-layer-transition grit caused essentially no change in the pitching-moment characteristics (figs. 10 and 11).

Drag.- The data for pressure drag and profile drag generally show the expected decrease in drag with increases in Reynolds number associated with the related decreases in boundary-layer thickness (fig. 10). At $M = 0.15$ and $c_l = 0.40$, the minimum value of $c_{d,w}$ at $R = 2.0 \times 10^6$ was about the same as the minimum value at $R = 17.0 \times 10^6$ (fig. 10(a)). The reason for this is the long region of laminar flow over the airfoil lower surface. A favorable pressure gradient exists back to about 0.08c and a zero gradient back to about 0.20c. (See fig. 7(a).) At negative angles of attack ($c_l < 0.4$) the drag increases as a result of transition to turbulent flow on the airfoil lower surface. Figure 7(a) shows the minimum pressure peak occurring at about 0.06c on the airfoil lower surface at $\alpha = -3.83°$. The upper-surface boundary layer is turbulent behind the laminar separation bubble, as discussed earlier.

At $M = 0.22$ (fig. 10(b)) the minimum profile drag coefficient $c_{d,w}$ varied from about 0.0092 at $R = 5.6 \times 10^6$ to about 0.0076 at $R = 25.0 \times 10^6$ and the maximum lift-drag ratio correspondingly increased from 98 to 108. Figure 11(c) summarizes the effect on $c_{d,w}$ from applying a boundary-layer-transition strip on both surfaces on the airfoil varying from 0.05c to 0.25c from the leading edge of the airfoil. Applying grit at 0.05c increased $c_{d,w}$ throughout the lift-coefficient range. As the transition-strip location was moved rearward, the effect on profile drag coefficient rapidly decreased and essentially disappeared at the most rearward location.

Comparison of Wind-Tunnel and Flight Data

The low-speed two-dimensional pressure data of this investigation have been compared with the three-dimensional wind-tunnel and flight data of reference 3 for the 17-percent-thick supercritical airfoil on the T-2C airplane. The results are shown in figure 14 at approximately the same section normal-force coefficient. The three-dimensional wind-tunnel and flight data were obtained at the 40-percent-semispan station. A 0.09-scale model of the T-2C airplane was used for the wind-tunnel investigation in the Langley 8-foot transonic pressure tunnel. The overall pressure distributions from the two-dimensional and three-dimensional data share common features. The flight data, however, display larger peak negative values of pressure coefficient, and hence larger pressure recovery on the airfoil upper surface, than the two-dimensional data. The differences in the values of C_p between the two-dimensional and three-dimensional data indicate that the airfoil section of the airplane requires a substantially higher angle of

attack to produce the same section normal-force coefficient than the two-dimensional section. (See also fig. 15.)

The vortex-lattice program of reference 13 was used to obtain the theoretical load distributions for the planform of the flight configuration. Results of this program were used to correct the two-dimensional lift characteristics to three-dimensional characteristics as shown in figure 15 (three-dimensional data from ref. 3). A decrease in lift-curve slope from a two-dimensional value of 0.12 per degree to a three-dimensional value of about 0.085 per degree was obtained, which agrees well with the flight data and other three-dimensional wind-tunnel data.

CONCLUDING REMARKS

Wind-tunnel tests have been conducted to determine the low-speed two-dimensional aerodynamic characteristics of a 17-percent-thick supercritical airfoil. The results were compared with three-dimensional wind-tunnel and flight data. The tests were conducted over a Mach number range from 0.15 to 0.30. Reynolds number based on the airfoil chord was varied from 2.0×10^6 to 25.0×10^6. The following results were obtained from this investigation:

1. Maximum section lift coefficients greater than 2.0 were obtained at test Reynolds numbers above 5.0×10^6.

2. Maximum section lift coefficients increased rapidly at Reynolds numbers from 2.0×10^6 to 5.0×10^6.

3. A measurable decrease in maximum section lift coefficient occurred at a Mach number of 0.15 as the Reynolds number was increased from about 9.0×10^6 to 17.0×10^6.

4. The maximum section lift coefficient decreased about 10 percent (2.04 to 1.80) when the Mach number was increased from 0.22 to 0.30 and the stall became less abrupt; this results from the flow over the airfoil becoming supercritical.

5. The lift-curve slopes of the corrected two-dimensional data were in good agreement with the lift-curve slopes obtained from three-dimensional wind-tunnel and flight data.

Langley Research Center,
National Aeronautics and Space Administration,
Hampton, Va., May 26, 1972.

REFERENCES

1. Whitcomb, Richard T.; and Clark, Larry R.: An Airfoil Shape for Efficient Flight at Supercritical Mach Numbers. NASA TM X-1109, 1965.
2. Harris, Charles D.: Wind-Tunnel Investigation of Effects of Trailing-Edge Geometry on a NASA Supercritical Airfoil Section. NASA TM X-2336, 1971.
3. Palmer, W. E.; Elliott, D. W.; and White, J. E.: Flight and Wind-Tunnel Evaluation of a 17% Thick Supercritical Airfoil on a T-2C Airplane, Vols. I and II. NR71H-150 (Navy Contract N00019-70-C-0474), North American Rockwell Corp., July 31, 1971.
4. Von Doenhoff, Albert E.; and Abbott, Frank T., Jr.: The Langley Two-Dimensional Low-Turbulence Pressure Tunnel. NACA TN 1283, 1947.
5. Braslow, Albert L.; and Knox, Eugene C.: Simplified Method for Determination of Critical Height of Distributed Roughness Particles for Boundary-Layer Transition at Mach Numbers From 0 to 5. NACA TN 4363, 1958.
6. Baals, Donald D.; and Mourhess, Mary J.: Numerical Evaluation of the Wake-Survey Equations for Subsonic Flow Including the Effect of Energy Addition. NACA WR L-5, 1945. (Formerly NACA ARR L5H27.)
7. Allen, H. Julian; and Vincenti, Walter G.: Wall Interference in a Two-Dimensional-Flow Wind Tunnel, With Consideration of the Effects of Compressibility. NACA Rep. 782, 1944. (Supersedes NACA WR A-63.)
8. Schlichting, Hermann (J. Kestin, transl.): Boundary Layer Theory. McGraw-Hill Book Co., Inc., 1955.
9. McCullough, George B.; and Gault, Donald E.: Examples of Three Representative Types of Airfoil-Section Stall at Low Speed. NACA TN 2502, 1951.
10. Loftin, Laurence K., Jr.; and Bursnall, William J.: The Effects of Variations in Reynolds Number Between 3.0×10^6 and 25.0×10^6 Upon the Aerodynamic Characteristics of a Number of NACA 6-Series Airfoil Sections. NACA Rep. 964, 1950. (Supersedes NACA TN 1773.)
11. Jacobs, Eastman N.; and Sherman, Albert: Airfoil Section Characteristics as Affected by Variations of the Reynolds Number. NACA Rep. 586, 1937.
12. Von Kármán, Th.: Compressibility Effects in Aerodynamics. J. Aeronaut. Sci., vol. 8, no. 9, July 1941, pp. 337-356.
13. Margason, Richard J.; and Lamar, John E.: Vortex Lattice FORTRAN Program for Estimating Subsonic Aerodynamic Characteristics of Complex Planforms. NASA TN D-6142, 1971.

14. Abbott, Ira H.; Von Doenhoff, Albert E.; and Stivers, Louis S., Jr.: Summary of Airfoil Data. NACA Rep. 824, 1945. (Supersedes NACA WR L-560.)

TABLE I.- SUPERCRITICAL AIRFOIL COORDINATES

[Leading-edge radius, 0.0428c; c = 58.42 cm (23 in.)]

x/c	$(z/c)_{upper}$	$(z/c)_{lower}$
0.0	0.000	0.000
.0125	.0304	-.030
.0250	.0401	-.0408
.0375	.0469	-.048
.0500	.0519	-.0533
.075	.0595	-.0611
.100	.0652	-.0664
.125	.06963	-.0704
.150	.07325	-.0735
.175	.07625	-.0760
.200	.07890	-.0779
.250	.0832	-.0807
.300	.0863	-.0819
.350	.08825	-.0820
.400	.0891	-.0810
.450	.08893	-.0786
.500	.08783	-.0748
.550	.08568	-.0690
.575	.08423	-.0652
.600	.08248	-.0607
.625	.08043	-.0554
.650	.07811	-.0495
.675	.07541	-.0431
.700	.07233	-.0366
.725	.06881	-.0301
.750	.06476	-.0240
.775	.0602	-.0184
.800	.0553	-.0134
.825	.0499	-.0093
.850	.0440	-.0060
.875	.0376	-.0036
.900	.0308	-.0021
.925	.0236	-.0017
.95	.0160	-.0025
.975	.0081	-.0044
1.000	.00	-.0080

TABLE II.- AIRFOIL ORIFICE LOCATIONS

Upper surface		Lower surface	
x/c	z/c	x/c	z/c
0.0062	0.0222	0.0000	-0.0014
.0127	.0305	.0054	-.0204
.0186	.0354	.0111	-.0244
.0245	.0396	.0177	-.0356
.0374	.0467	.0244	-.0406
.0497	.0517	.0370	-.0477
.0622	.0558	.0489	-.0530
.0752	.0594	.0610	-.0572
.0996	.0650	.0745	-.0611
.1493	.0731	.0988	-.0663
.1998	.0788	.1485	-.0736
.2501	.0831	.1989	-.0781
.2999	.0861	.2490	-.0810
.3503	.0880	.2982	-.0822
.3992	.0888	.3482	-.0823
.4505	.0886	.3980	-.0813
.5005	.0875	.4485	-.0789
.5503	.0854	.4482	-.0751
.6011	.0821	.5487	-.0692
.6506	.0778	.5989	-.0609
.7003	.0721	.6486	-.0498
.7503	.0645	.6990	-.0368
.8003	.0551	.7490	-.0242
.8498	.0438	.7993	-.0135
.8998	.0306	.8499	-.0661
.9496	.0160	.8499	-.0023
.9893	.0032	.9506	-.0028
		.9899	-.0066
		1.0000	-.0046

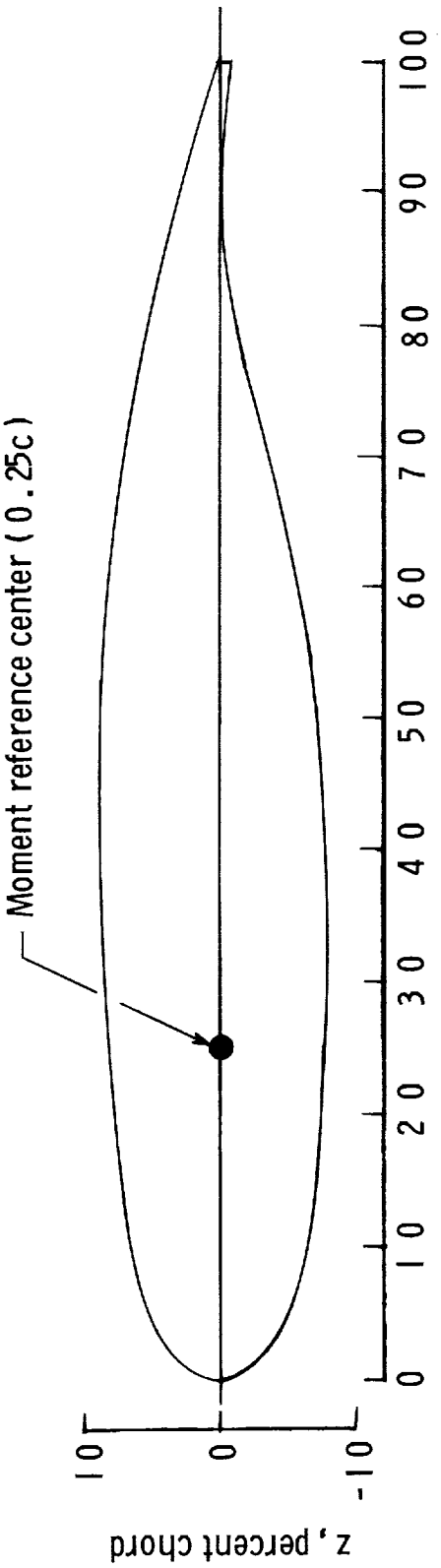

Figure 1.- Airfoil section shape.

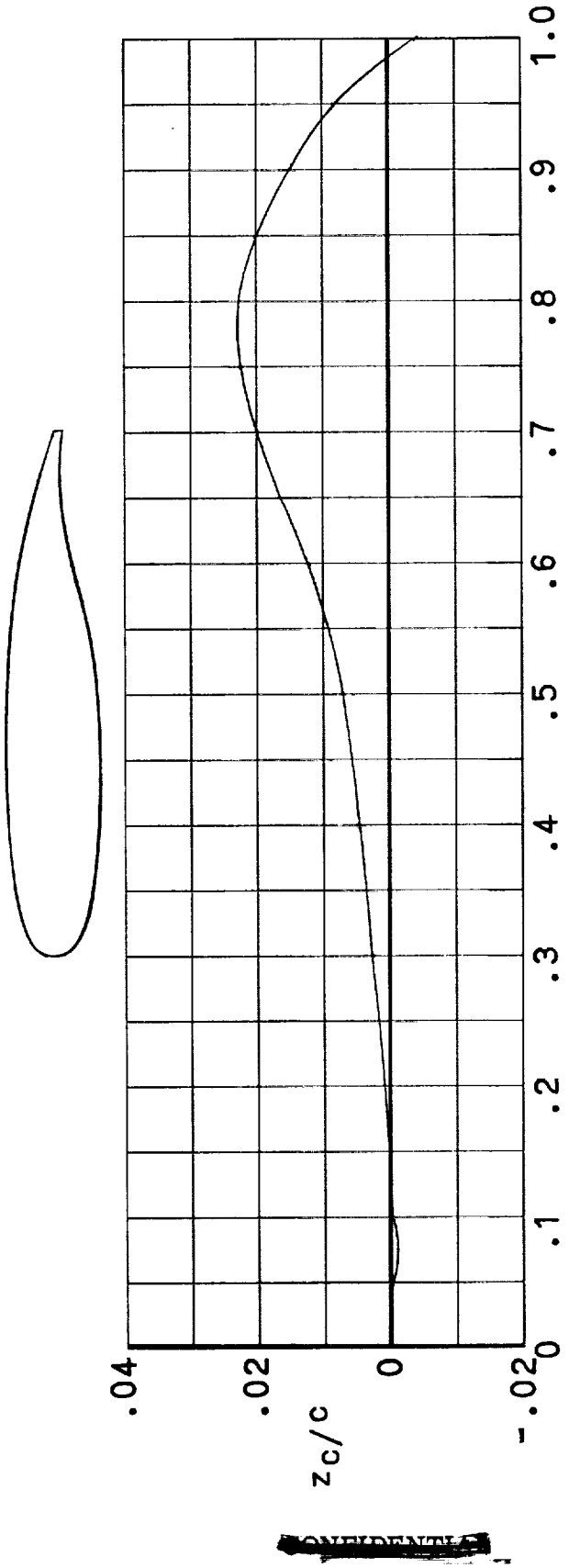

Figure 2.- Camber line for 17-percent-thick supercritical airfoil.

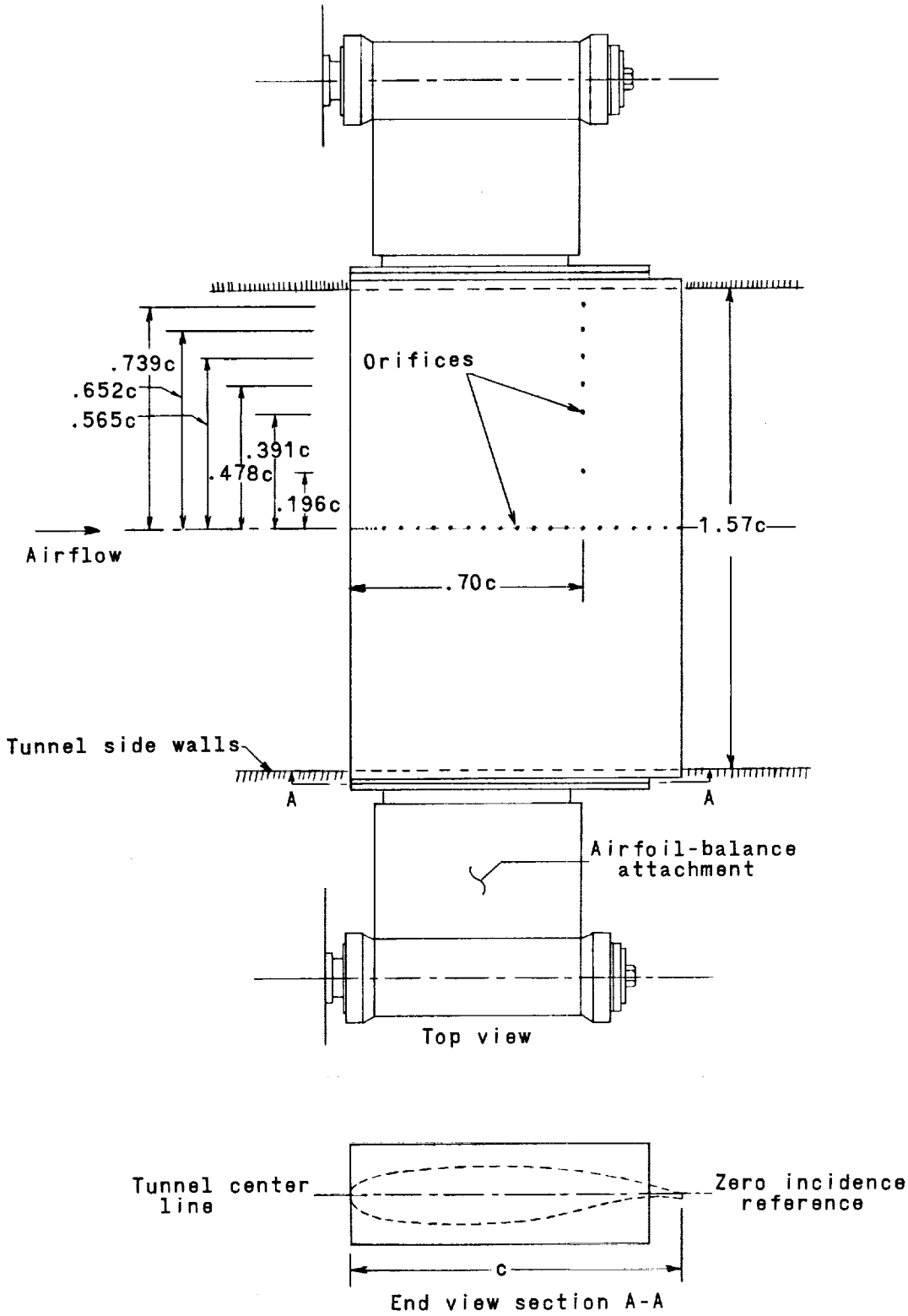

Figure 3.- Airfoil mounted in wind tunnel. All dimensions in terms of airfoil chord. c = 58.42 cm (23 in.).

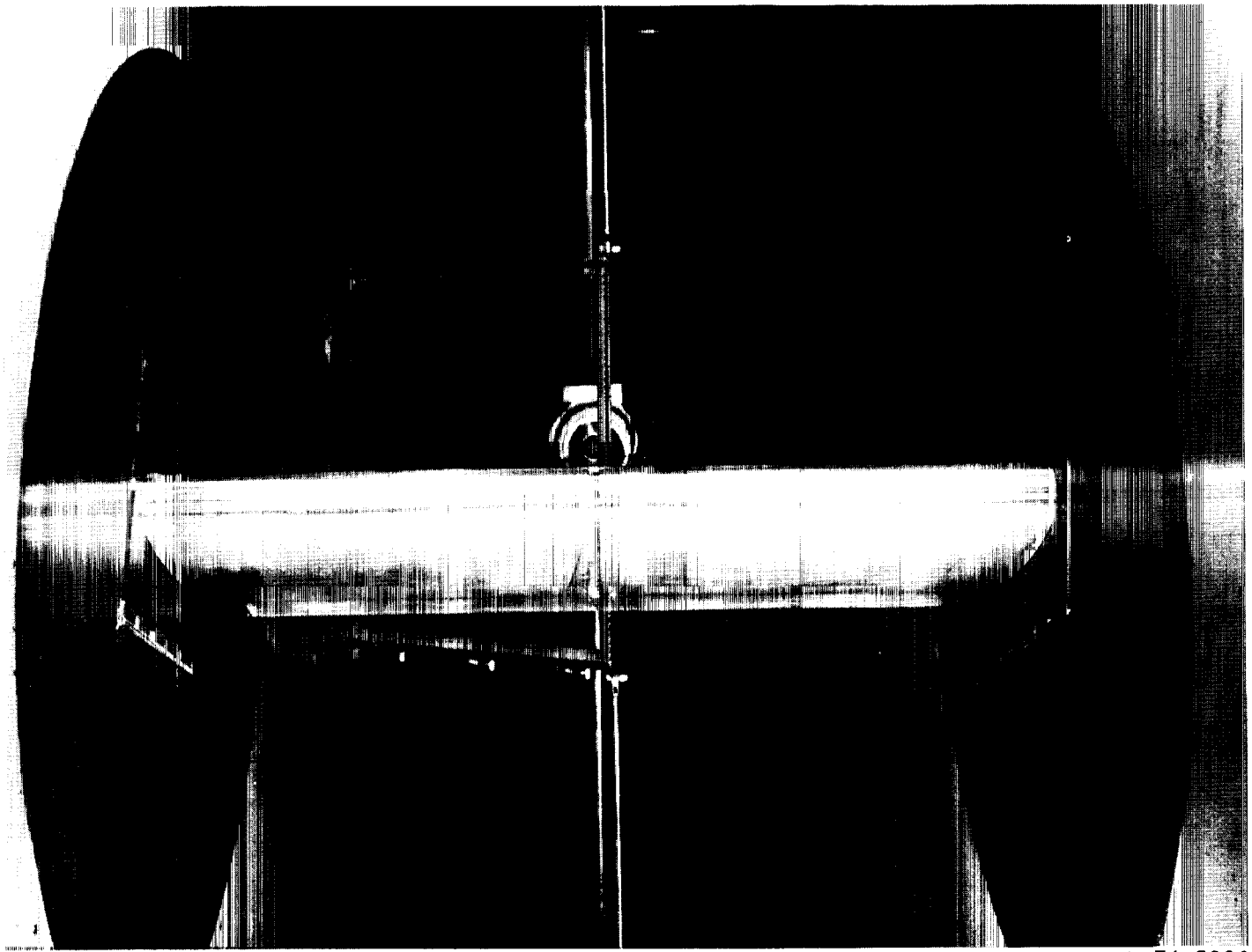

L-71-5286

Figure 4.- Photograph of airfoil mounted in wind tunnel.

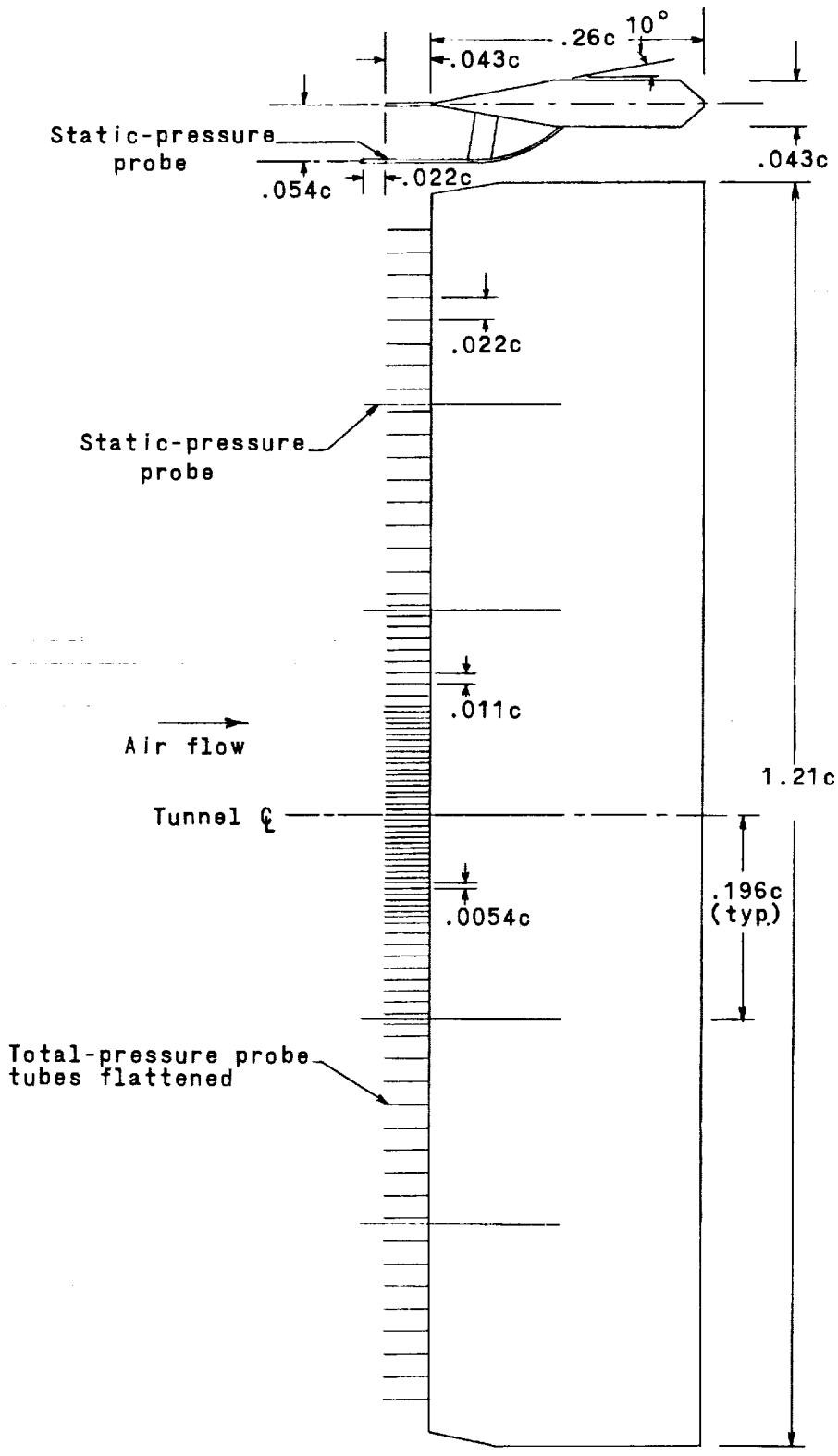

Figure 5.- Drawing of wake rake. All dimensions in terms of airfoil chord. c = 58.42 cm (23 in.).

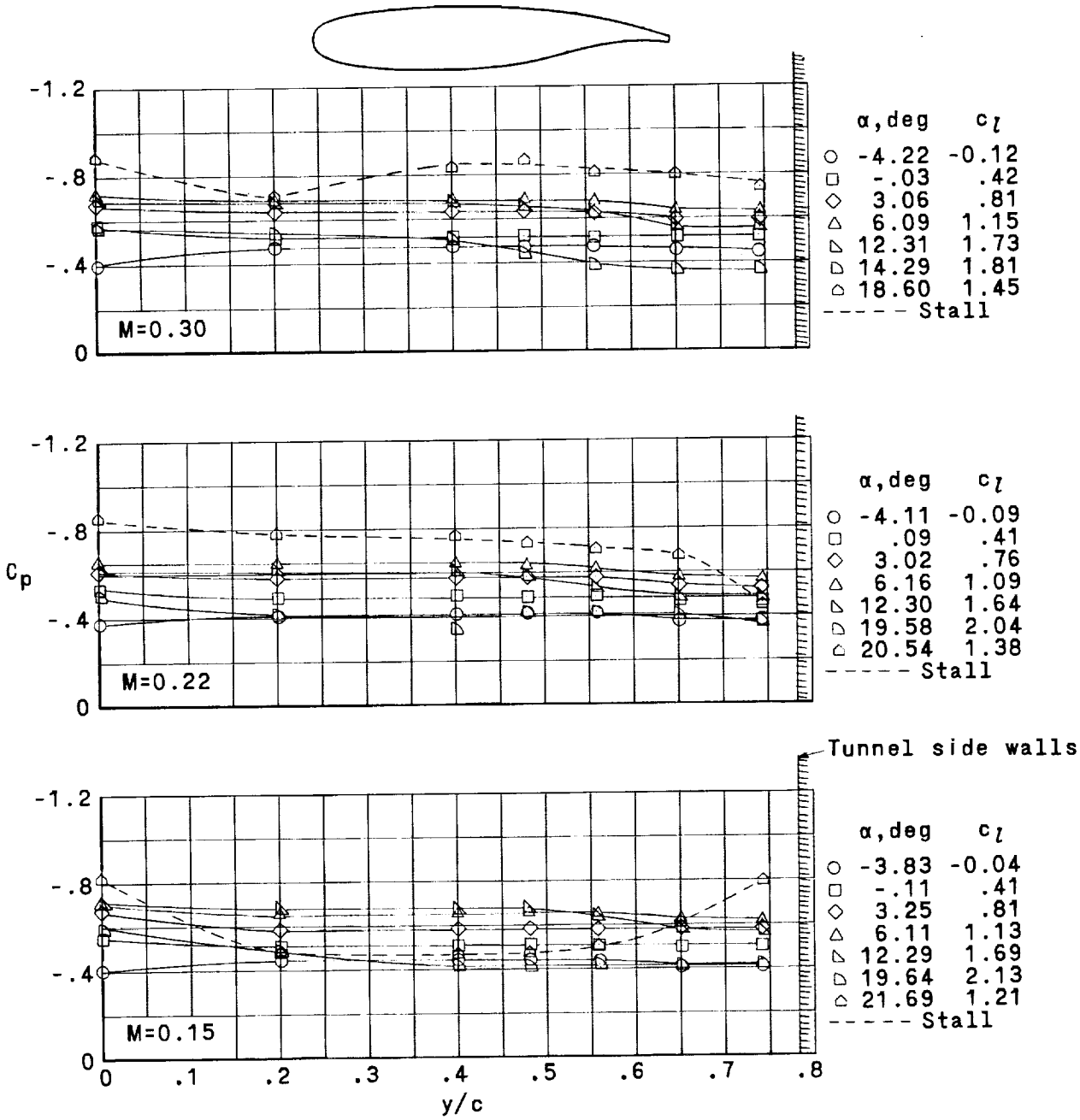

Figure 6.- Upper-surface spanwise pressure distributions for $x/c = 0.70$ and $R = 9.0 \times 10^6$.

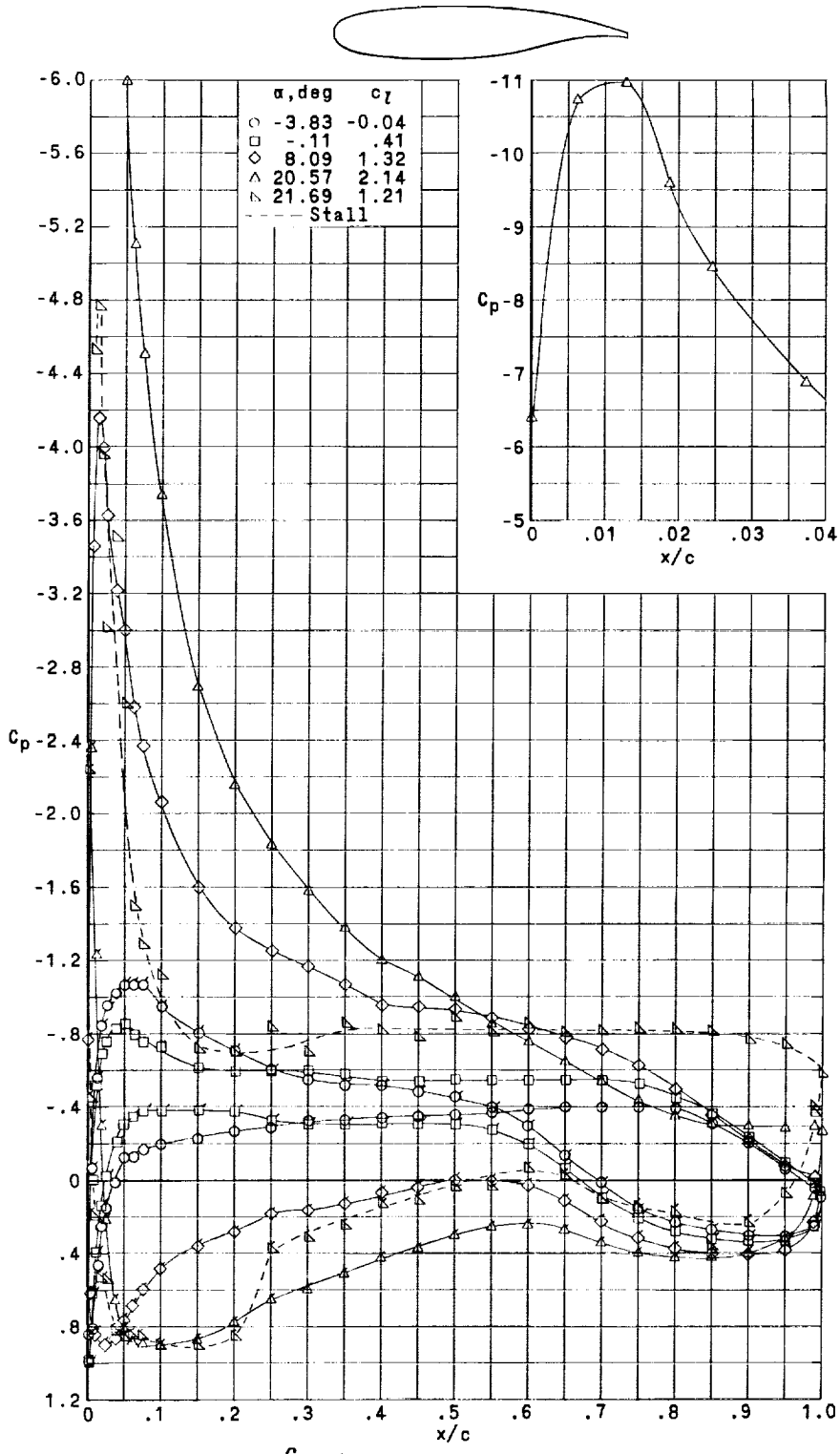

(a) M = 0.15; R = 9.3×10^6. (Flagged symbols indicate lower surface.)

Figure 7.- Effect of angle of attack and Mach number on chordwise pressure distributions.

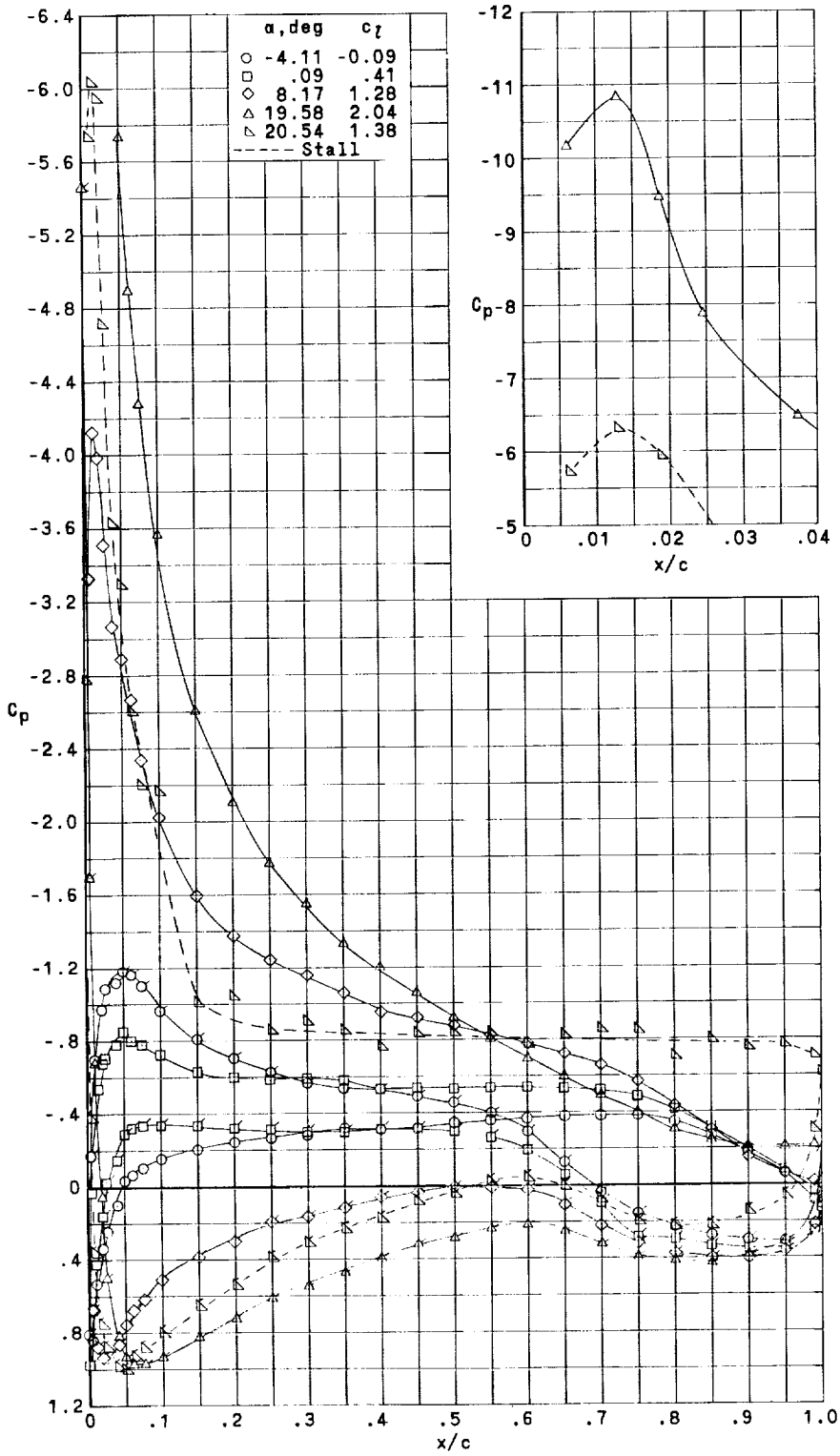

(b) M = 0.22; R = 9.4×10^6. (Flagged symbols indicate lower surface.)

Figure 7.- Continued.

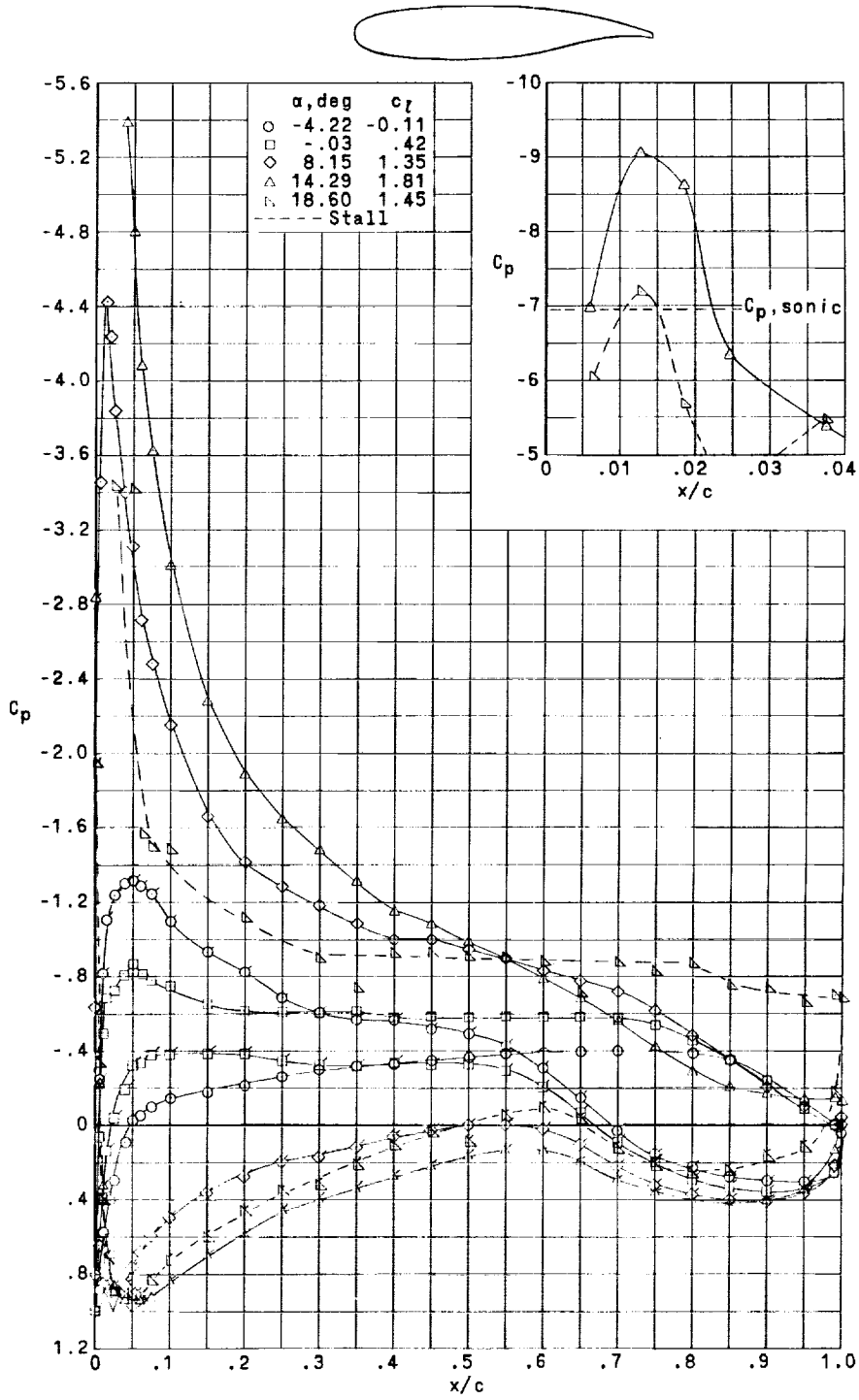

(c) M = 0.30; R = 9.4×10^6. (Flagged symbols indicate lower surface.)

Figure 7.- Concluded.

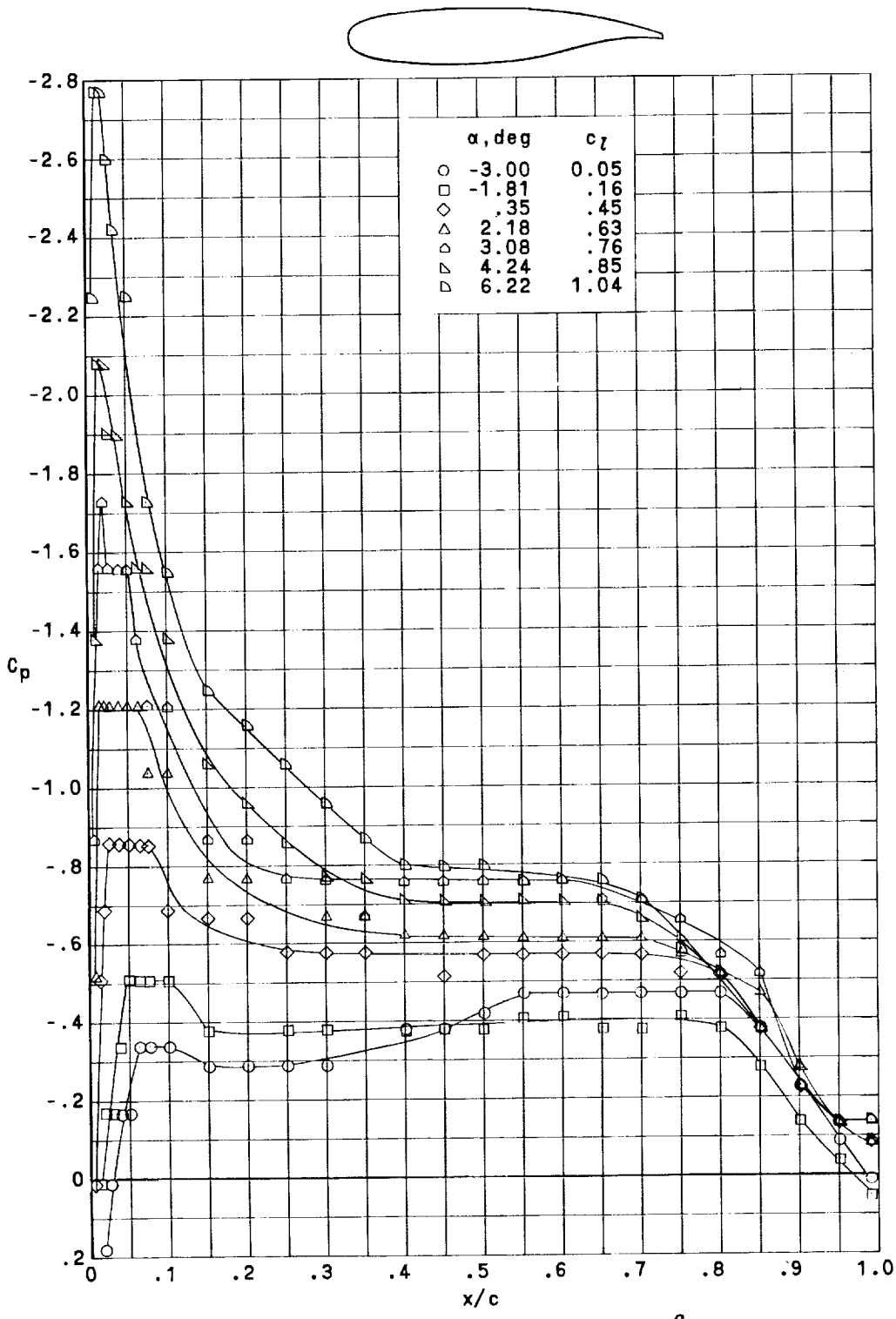

(a) Effect of angle of attack. $R = 2.0 \times 10^6$.

Figure 8.- Upper-surface pressure distributions illustrating effects of laminar separation bubble. M = 0.15.

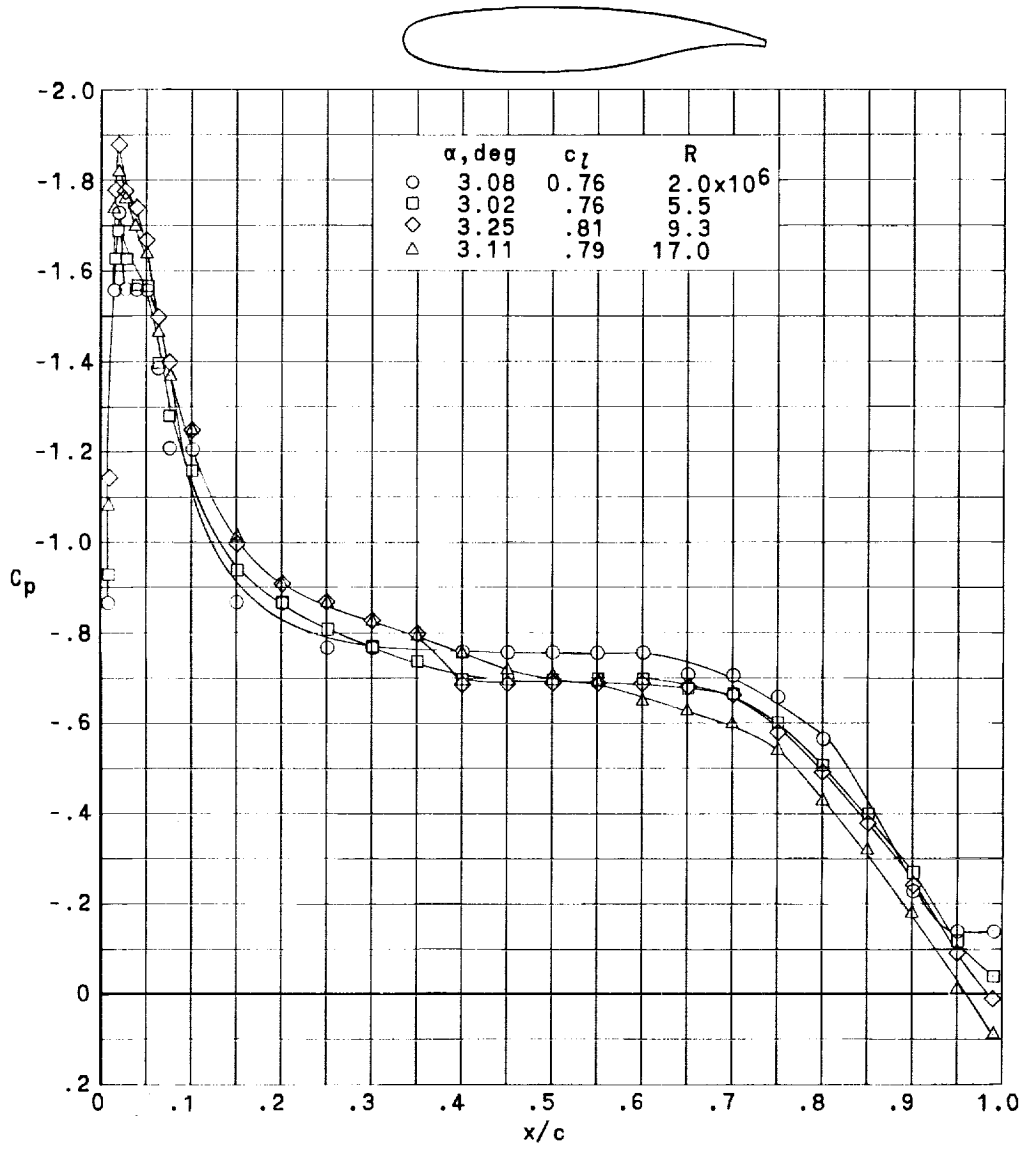

(b) Effect of Reynolds number. $\alpha \approx 3.0^{\circ}$.

Figure 8.- Concluded.

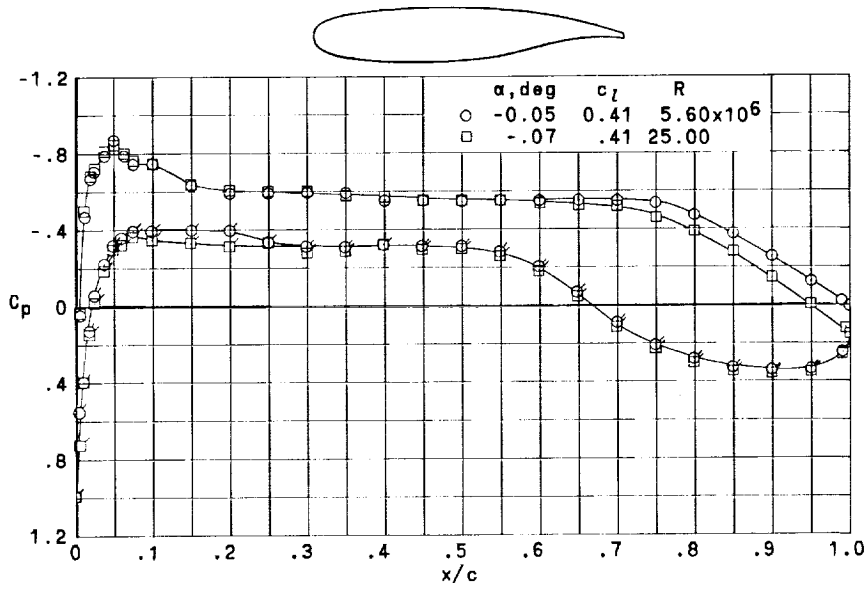

(a) M = 0.22; c_l = 0.41. (Flagged symbols indicate lower surface.)

Figure 9.- Effect of Reynolds number on the chordwise pressure distributions.

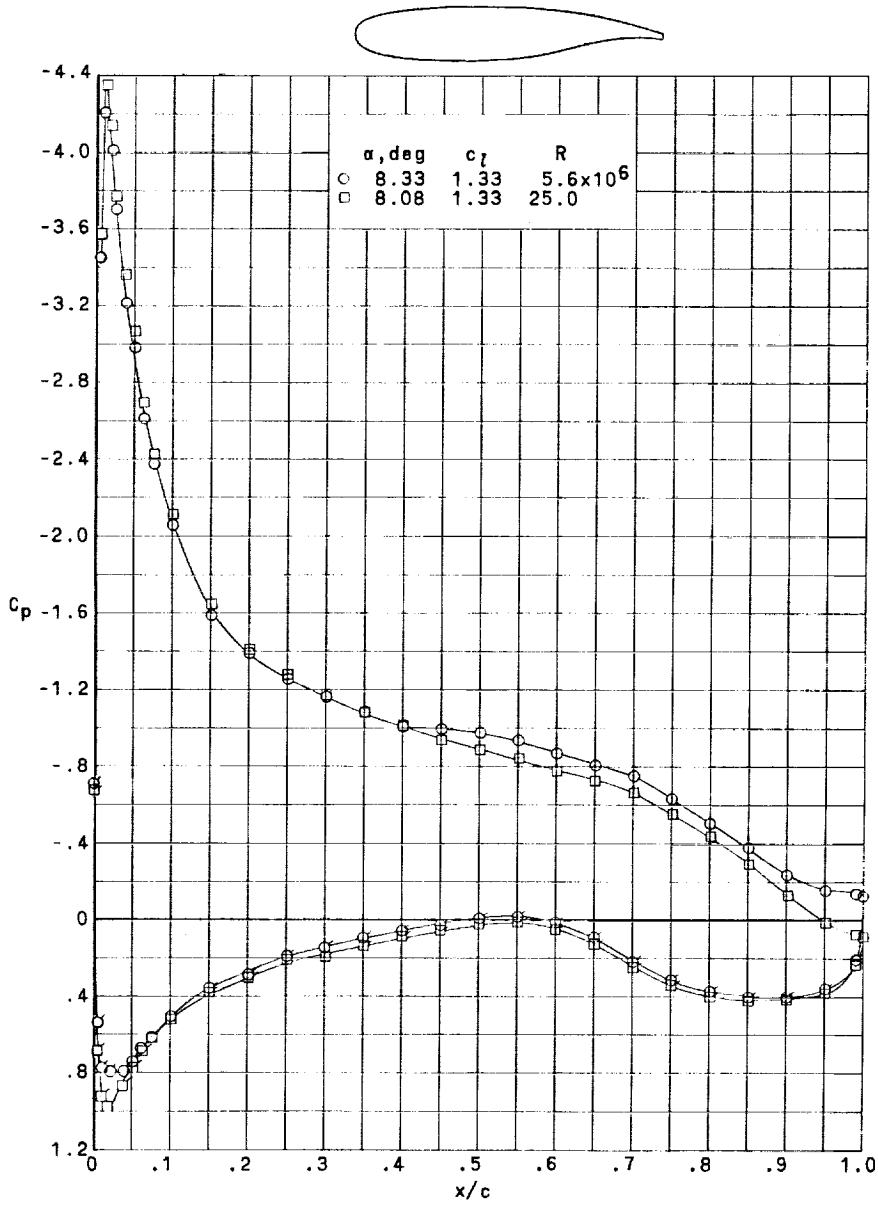

(b) M = 0.22; c_l = 1.33. (Flagged symbols indicate lower surface.)

Figure 9.- Continued.

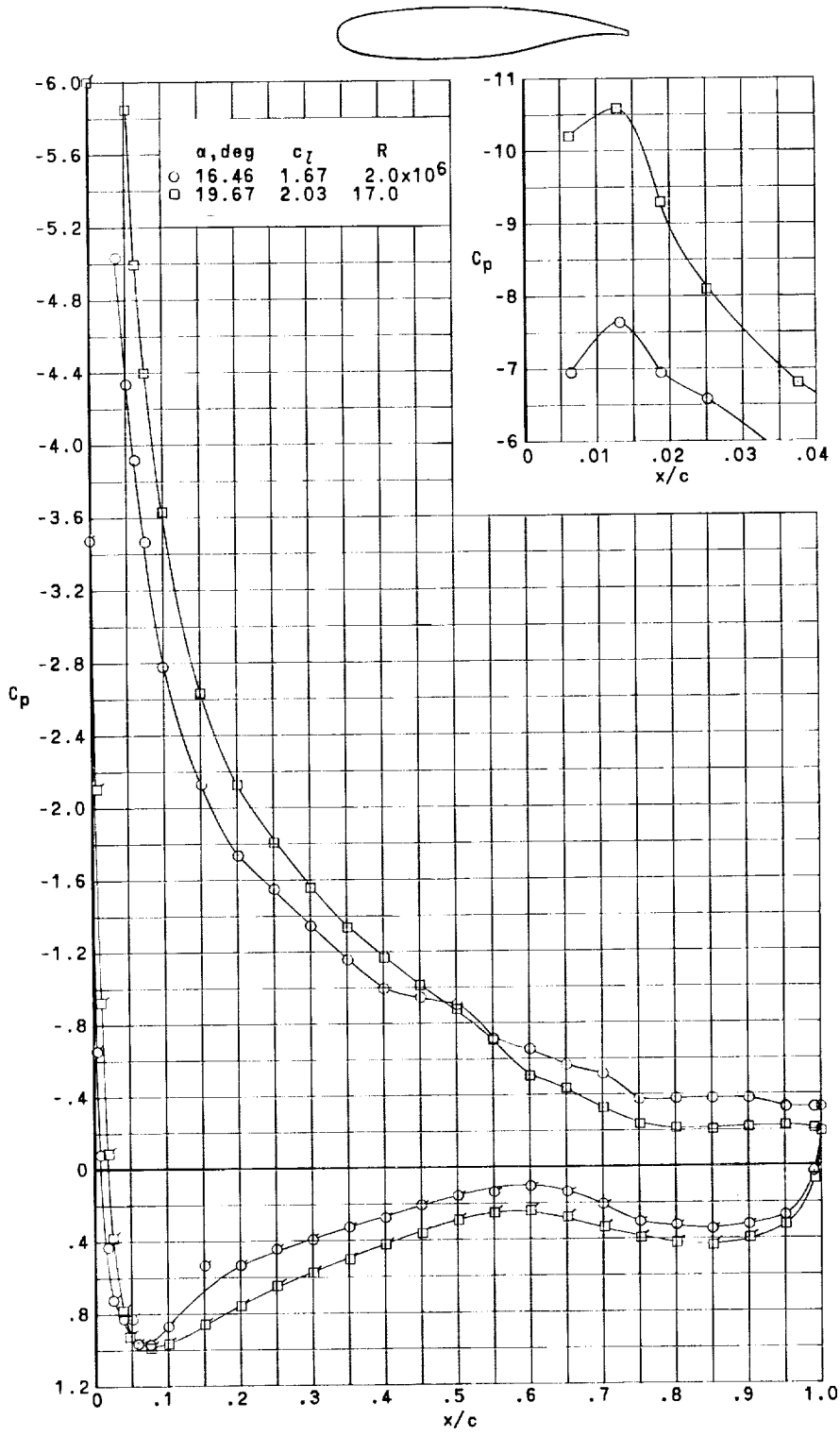

(c) M = 0.15; $c_l \approx (c_l)_{max}$. (Flagged symbols indicate lower surface.)

Figure 9.- Continued.

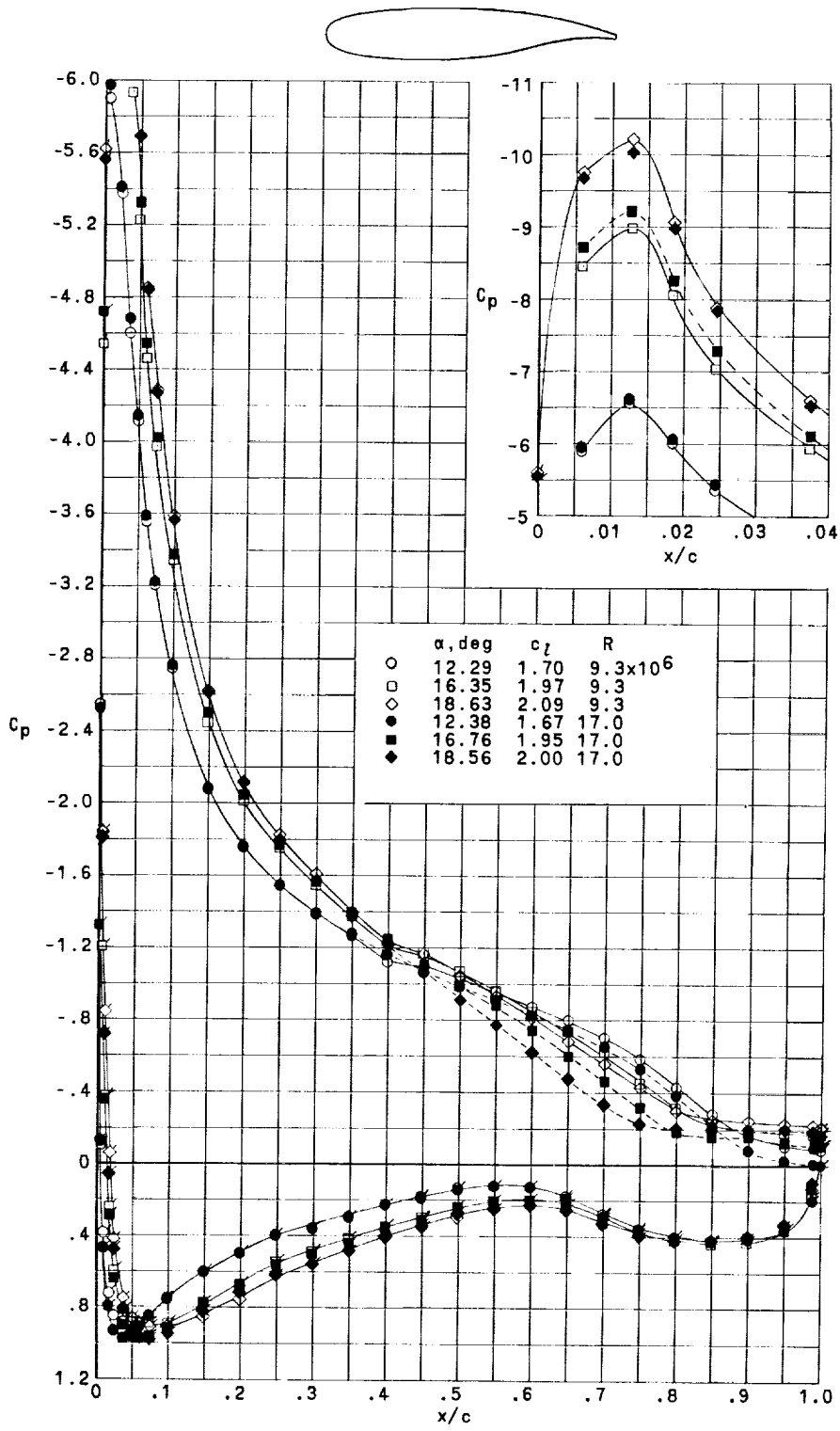

(d) M = 0.15. (Flagged symbols indicate lower surface.)

Figure 9.- Continued.

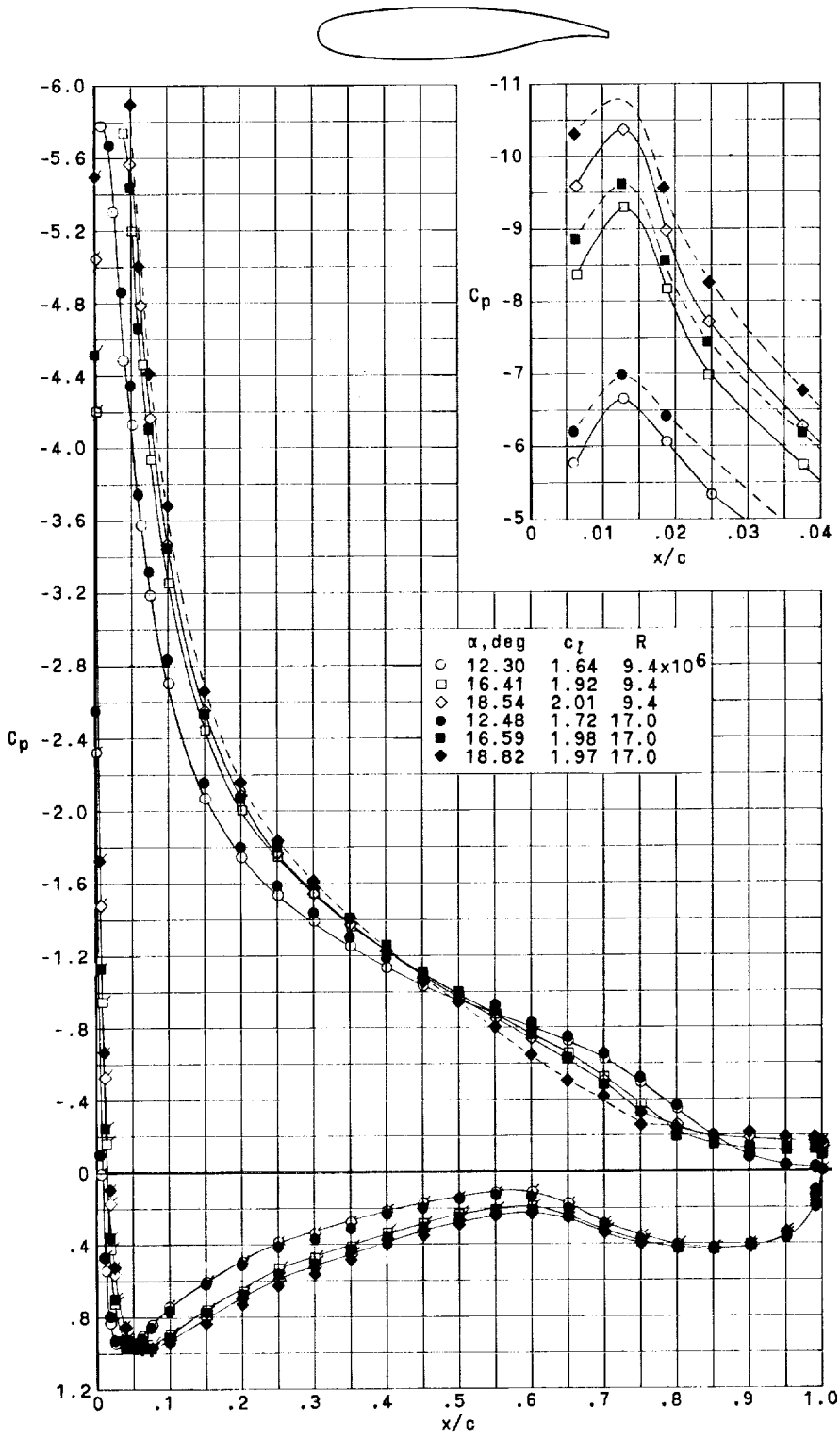

(e) M = 0.22. (Flagged symbols indicate lower surface.)

Figure 9.- Concluded.

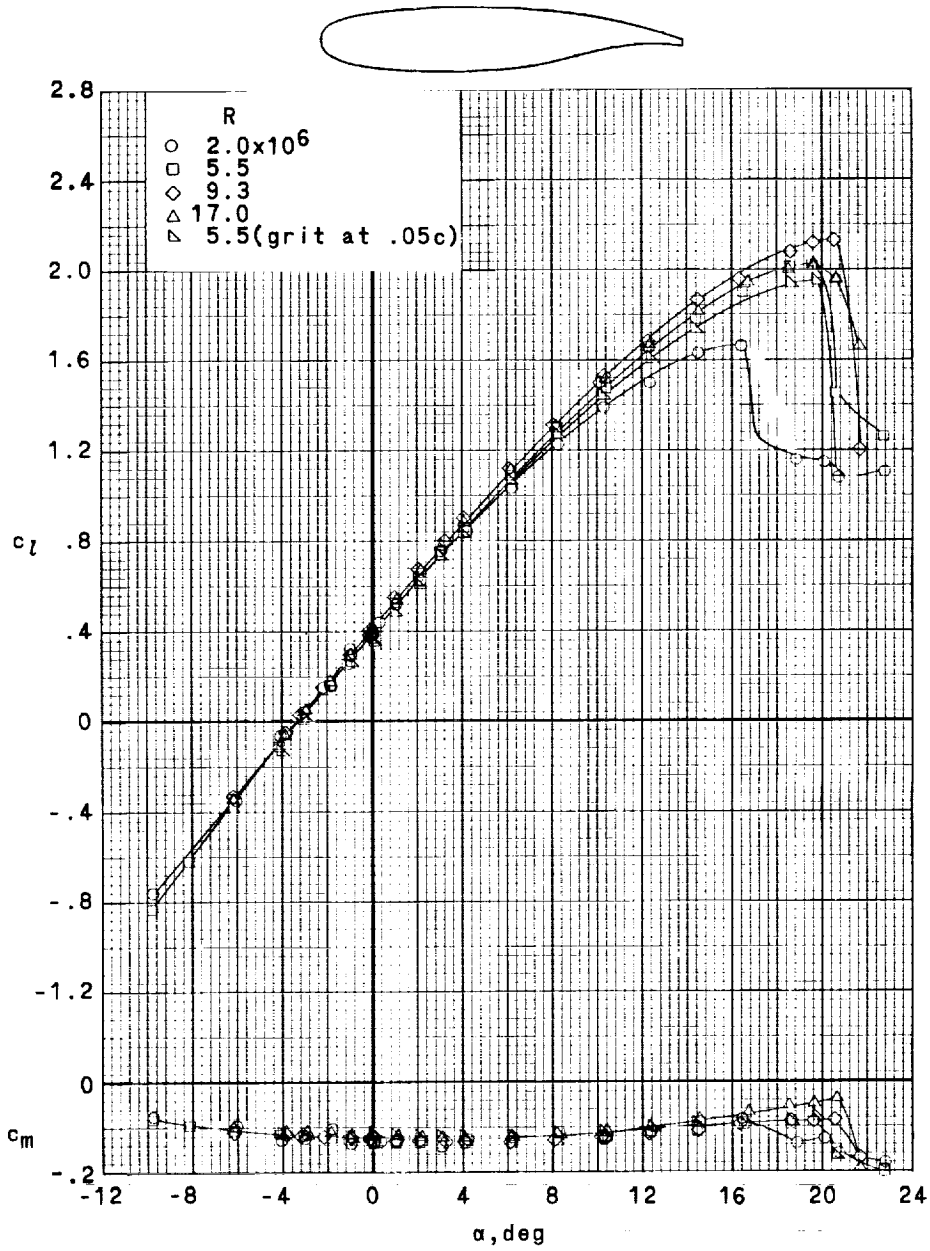

(a) M = 0.15.

Figure 10.- Two-dimensional section characteristics.

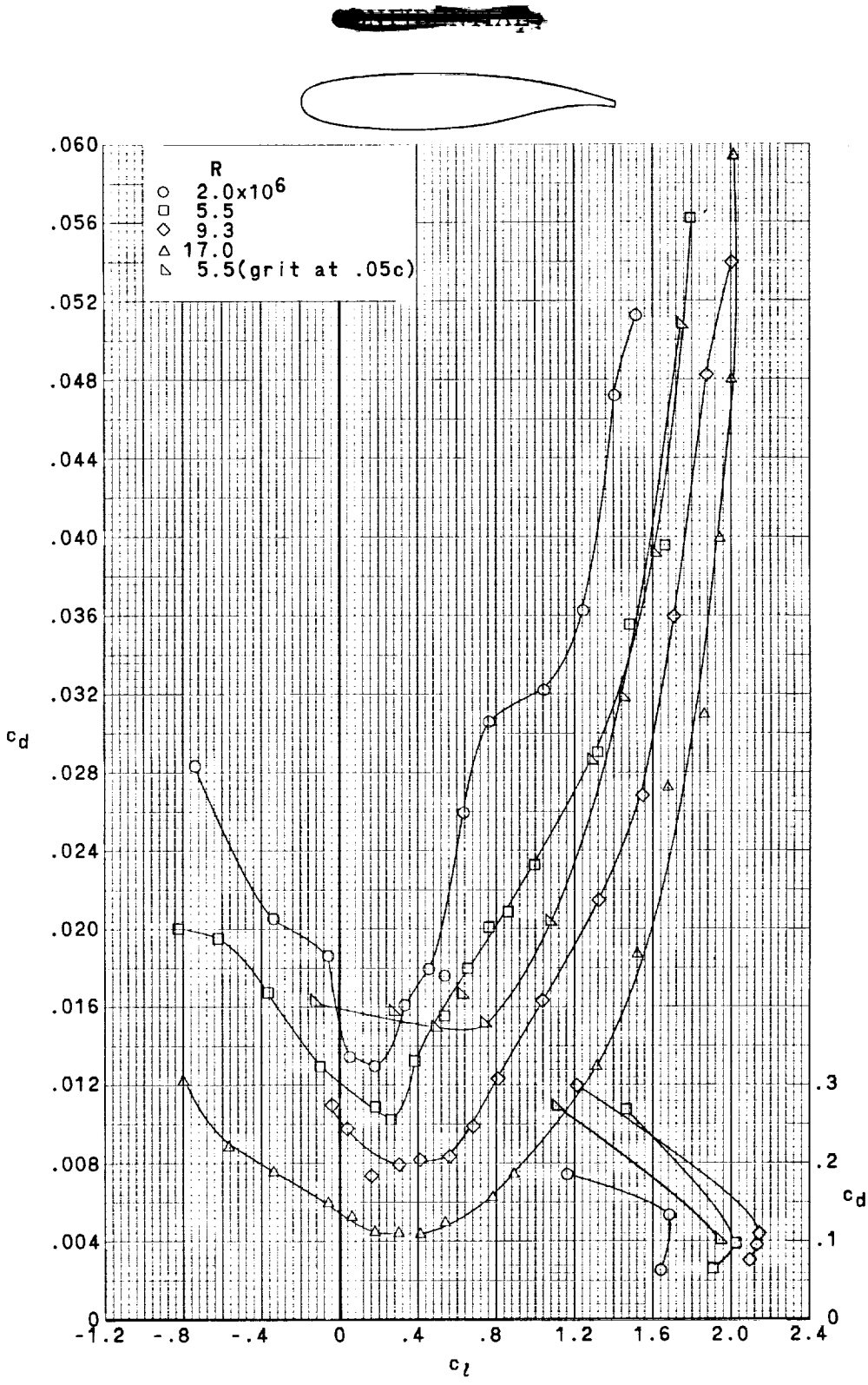

(a) M = 0.15. Continued.

Figure 10.- Continued.

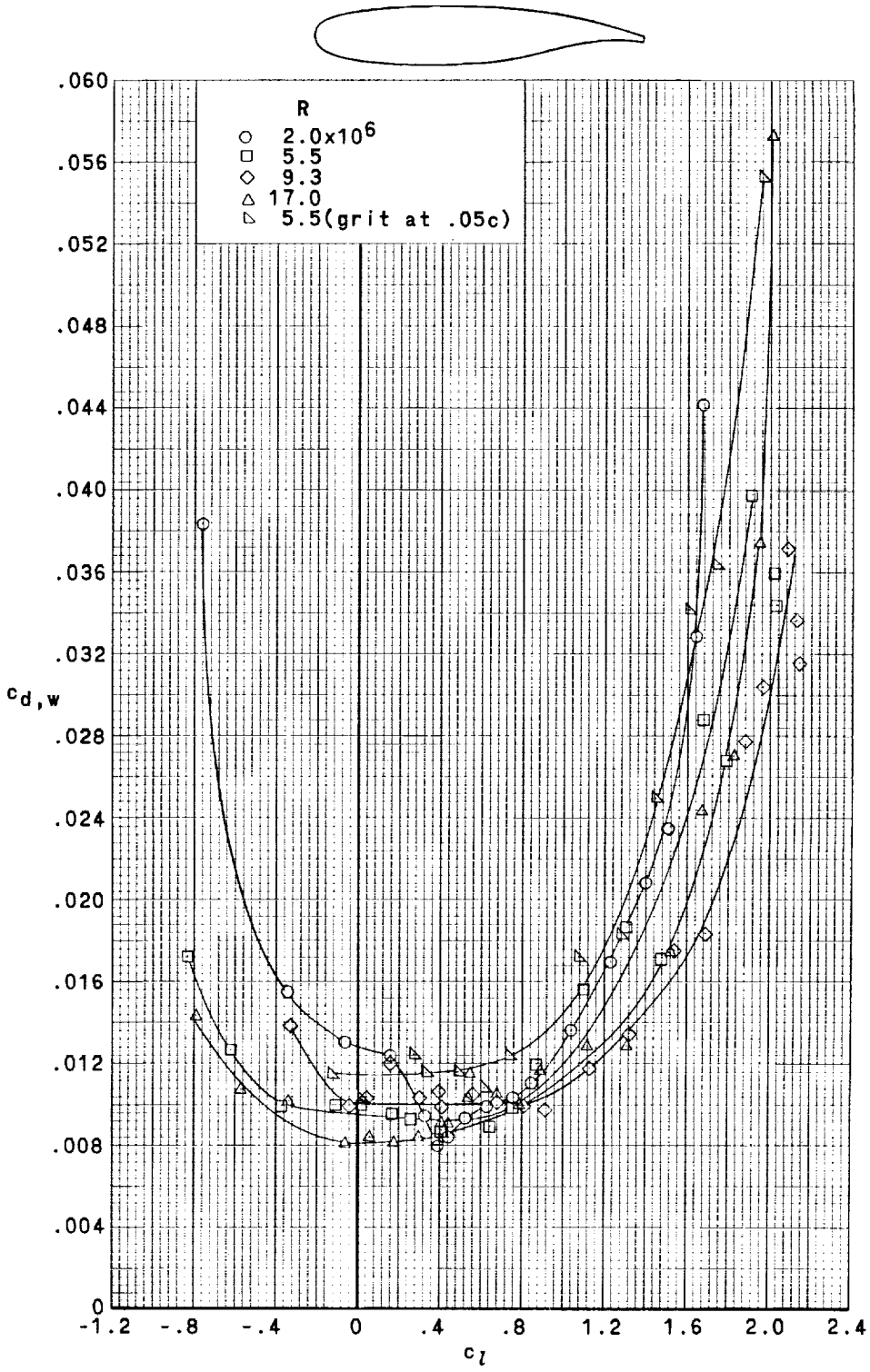

(a) M = 0.15. Concluded.

Figure 10.- Continued.

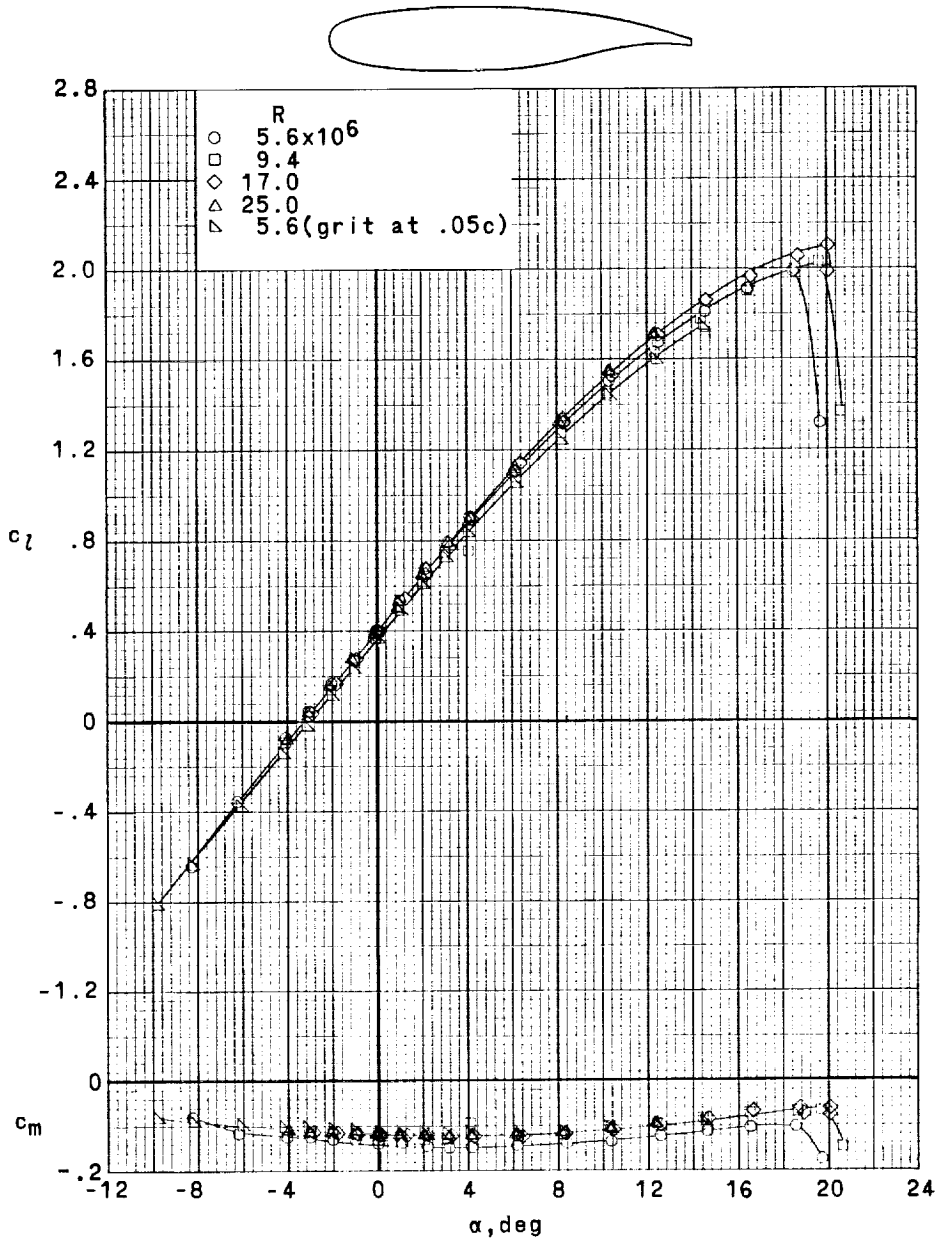

(b) M = 0.22.

Figure 10.- Continued.

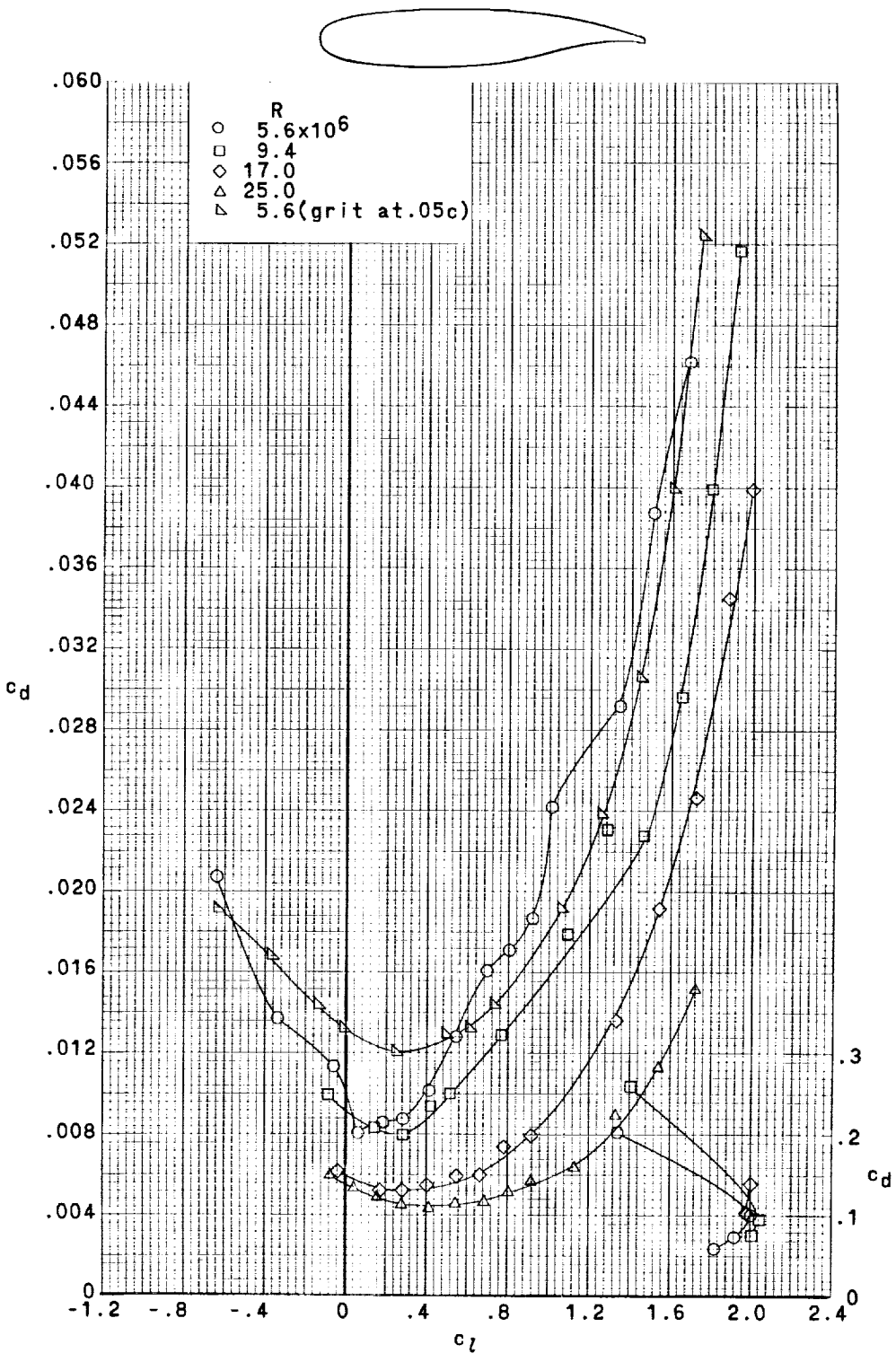

(b) M = 0.22. Continued.

Figure 10.- Continued.

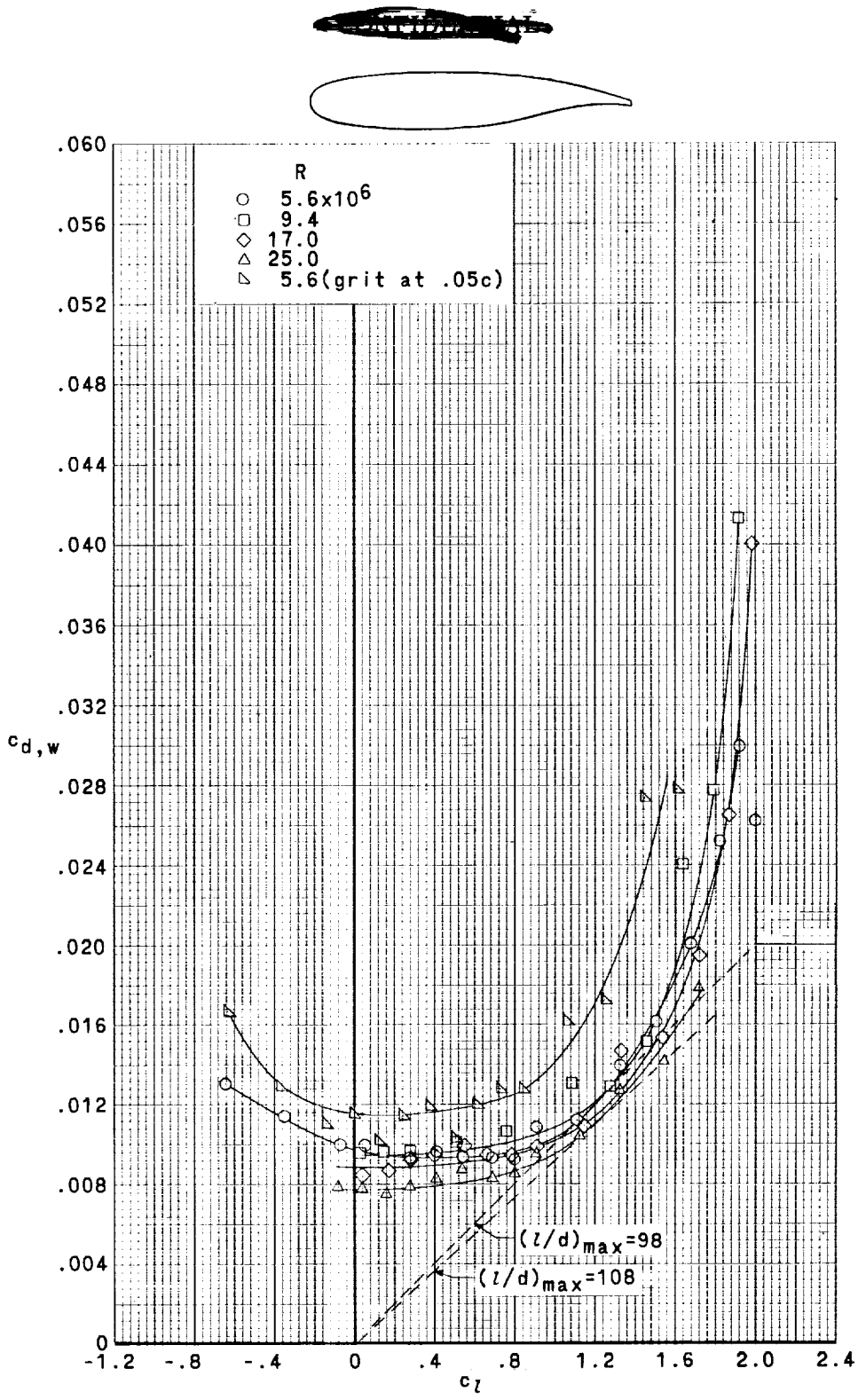

(b) M = 0.22. Concluded.

Figure 10.- Continued.

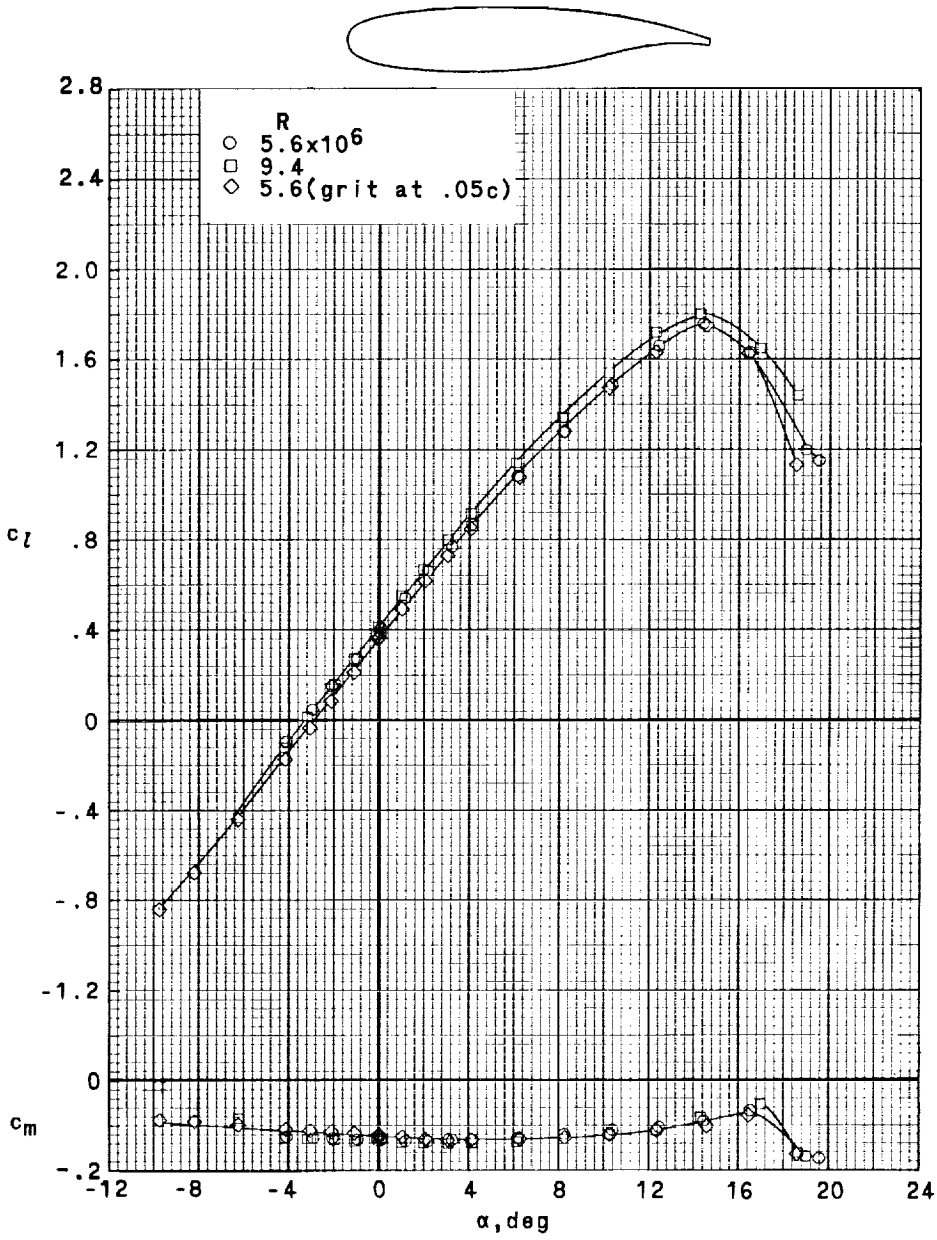

(c) M = 0.30.

Figure 10.- Continued.

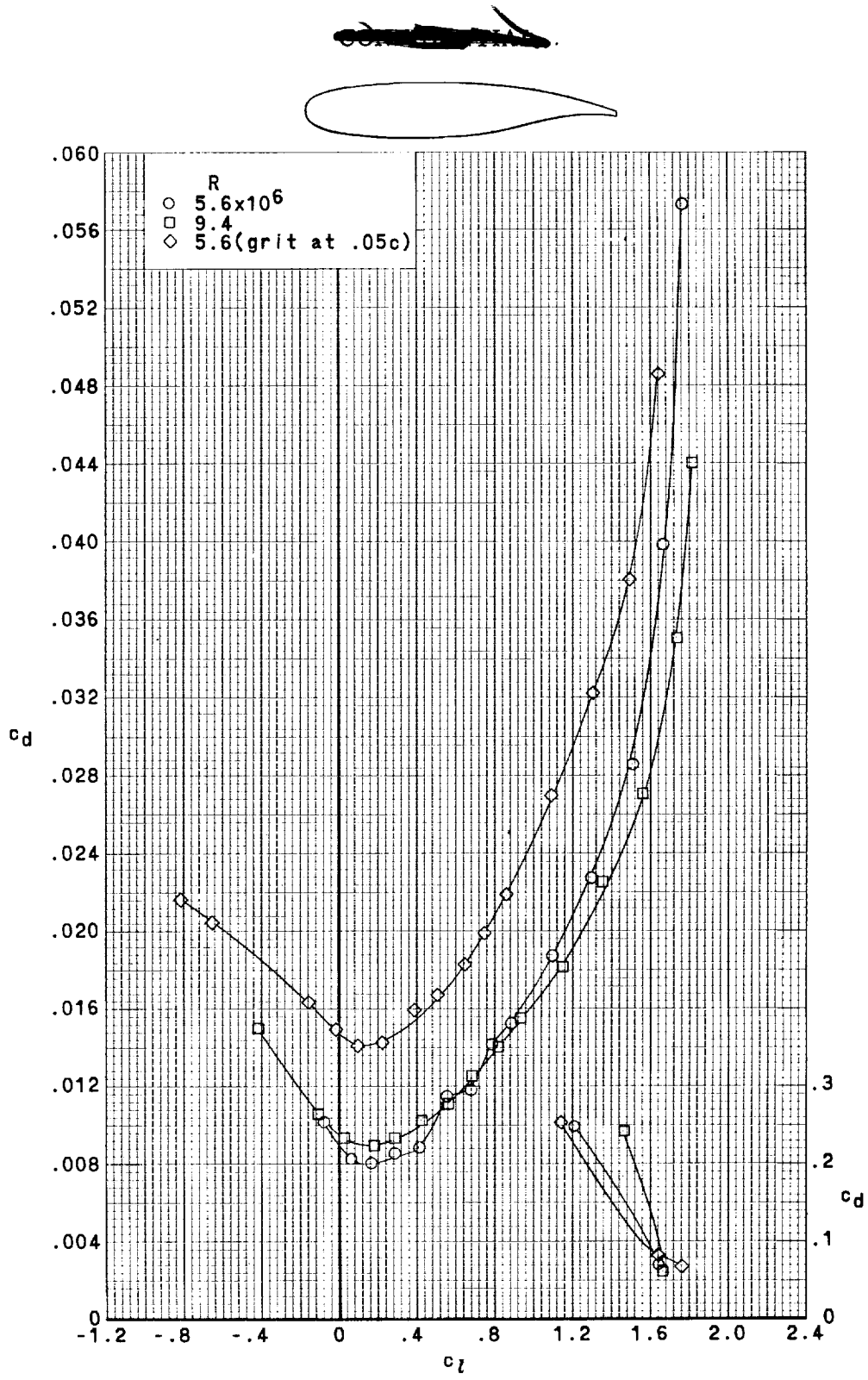

(c) M = 0.30. Continued.

Figure 10.- Continued.

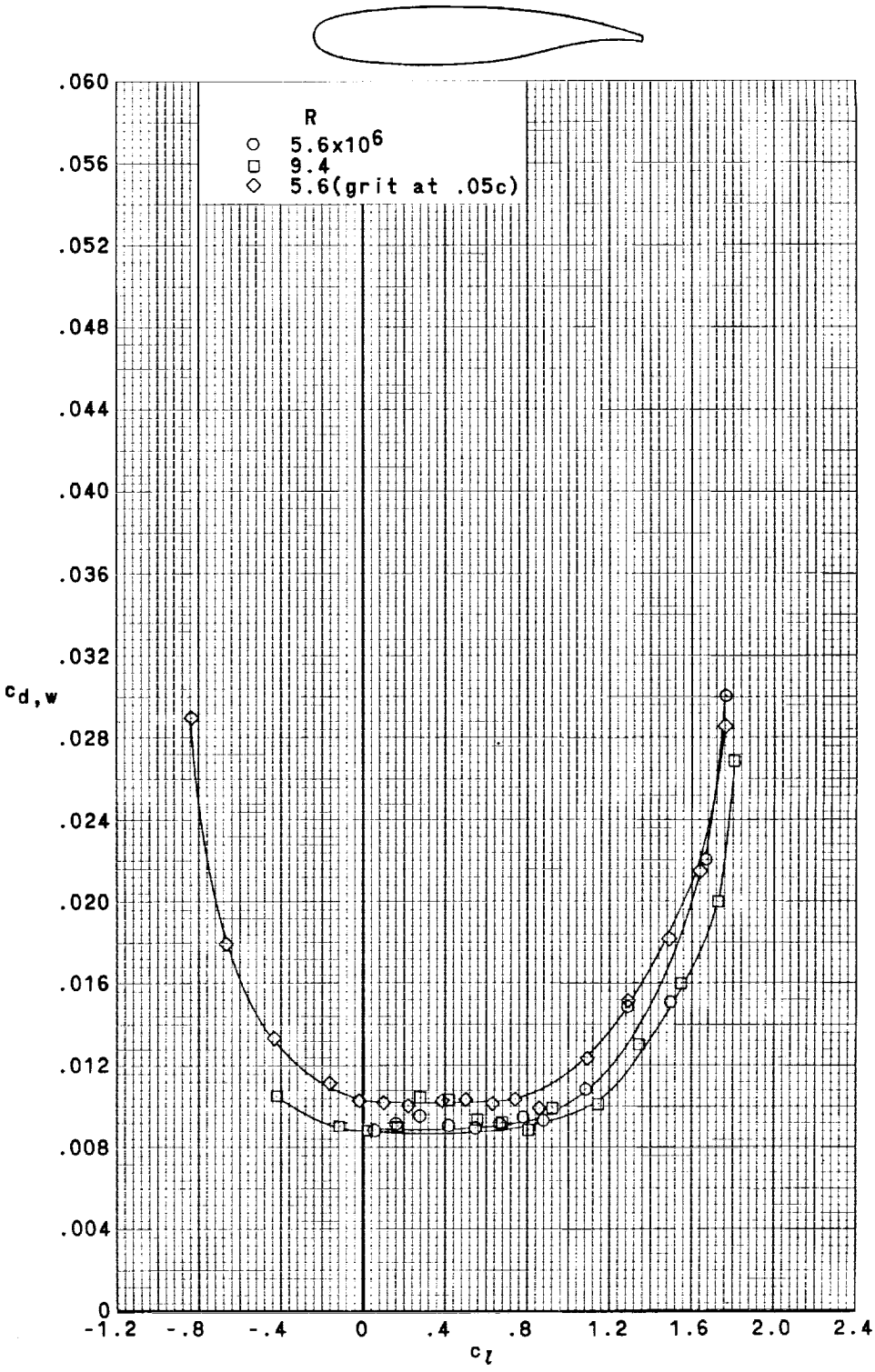

(c) M = 0.30. Concluded.

Figure 10.- Concluded.

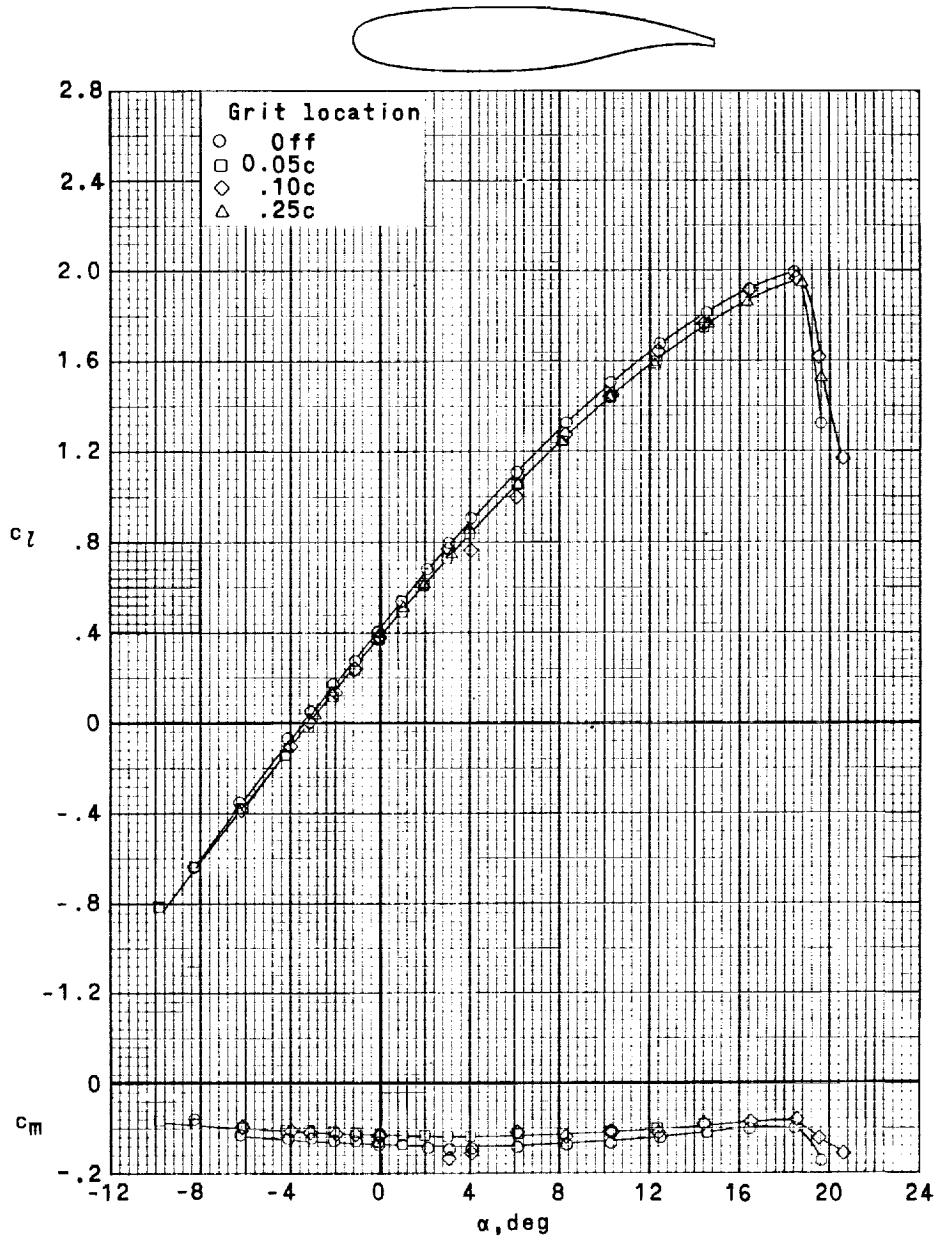

(a) c_l and c_m versus α.

Figure 11.- Effect of grit location on section characteristics.
M = 0.22; R = 5.6×10^6.

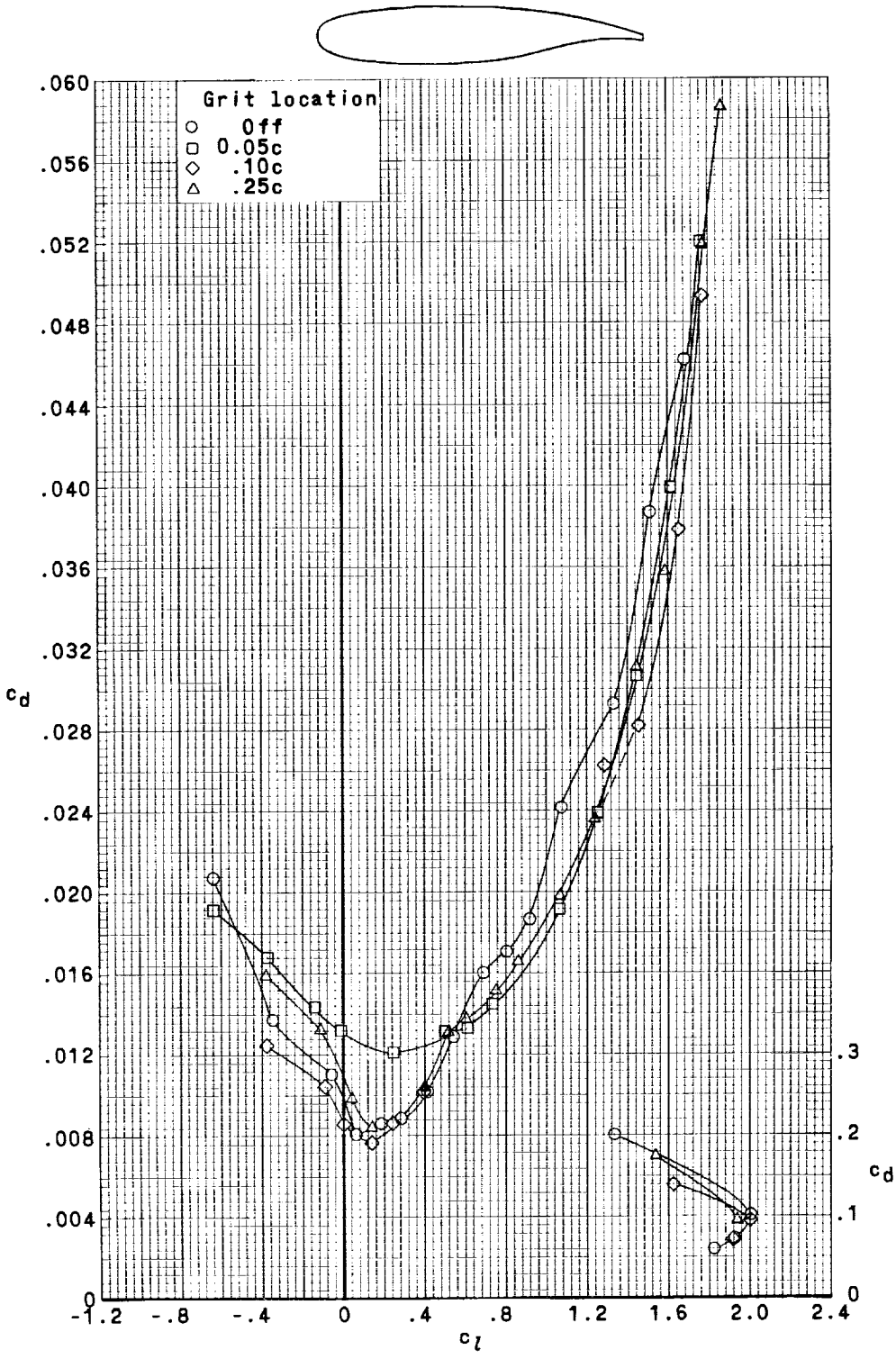

(b) c_d versus c_l.

Figure 11.- Continued.

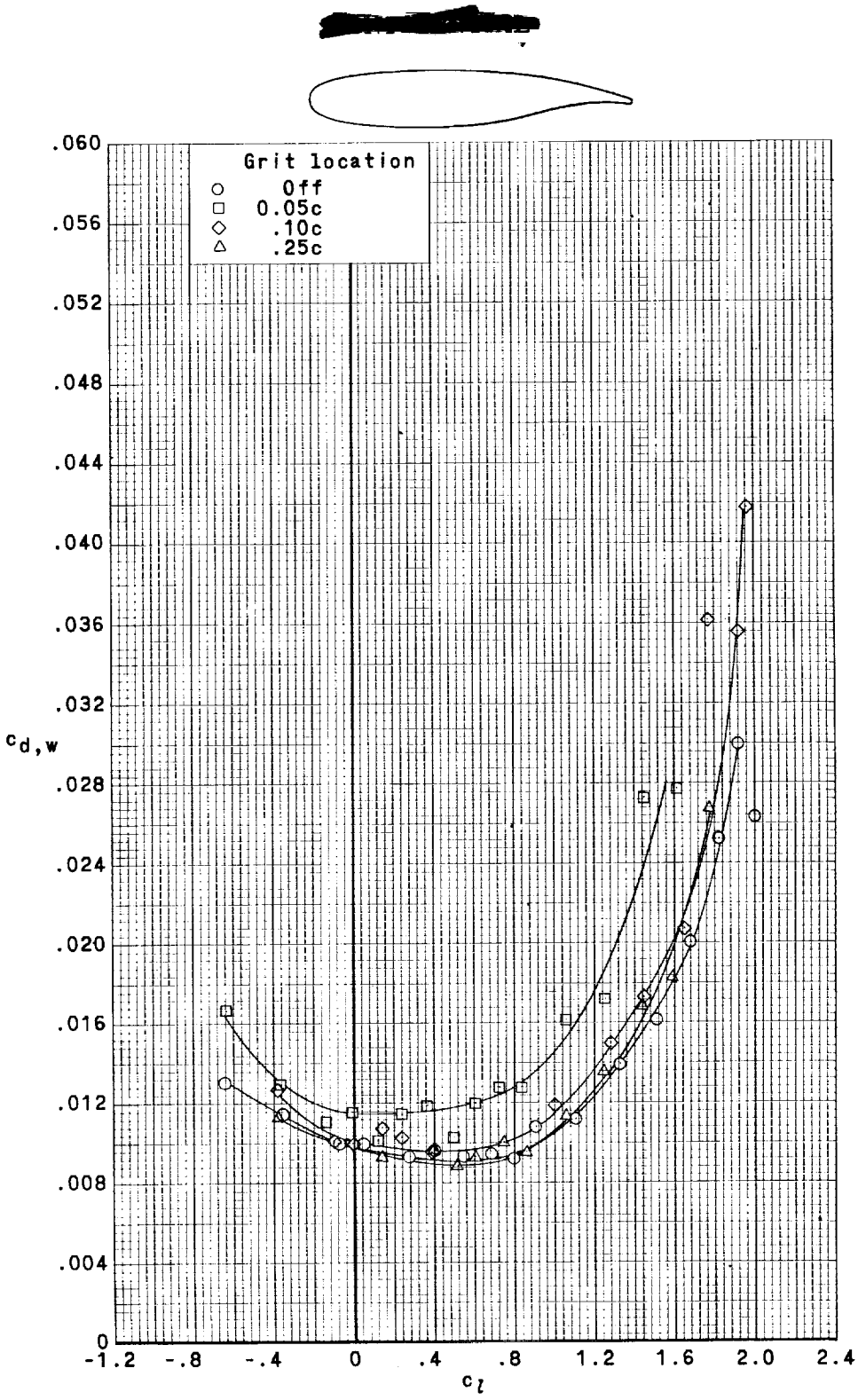

(c) $c_{d,w}$ versus c_l.

Figure 11.- Concluded.

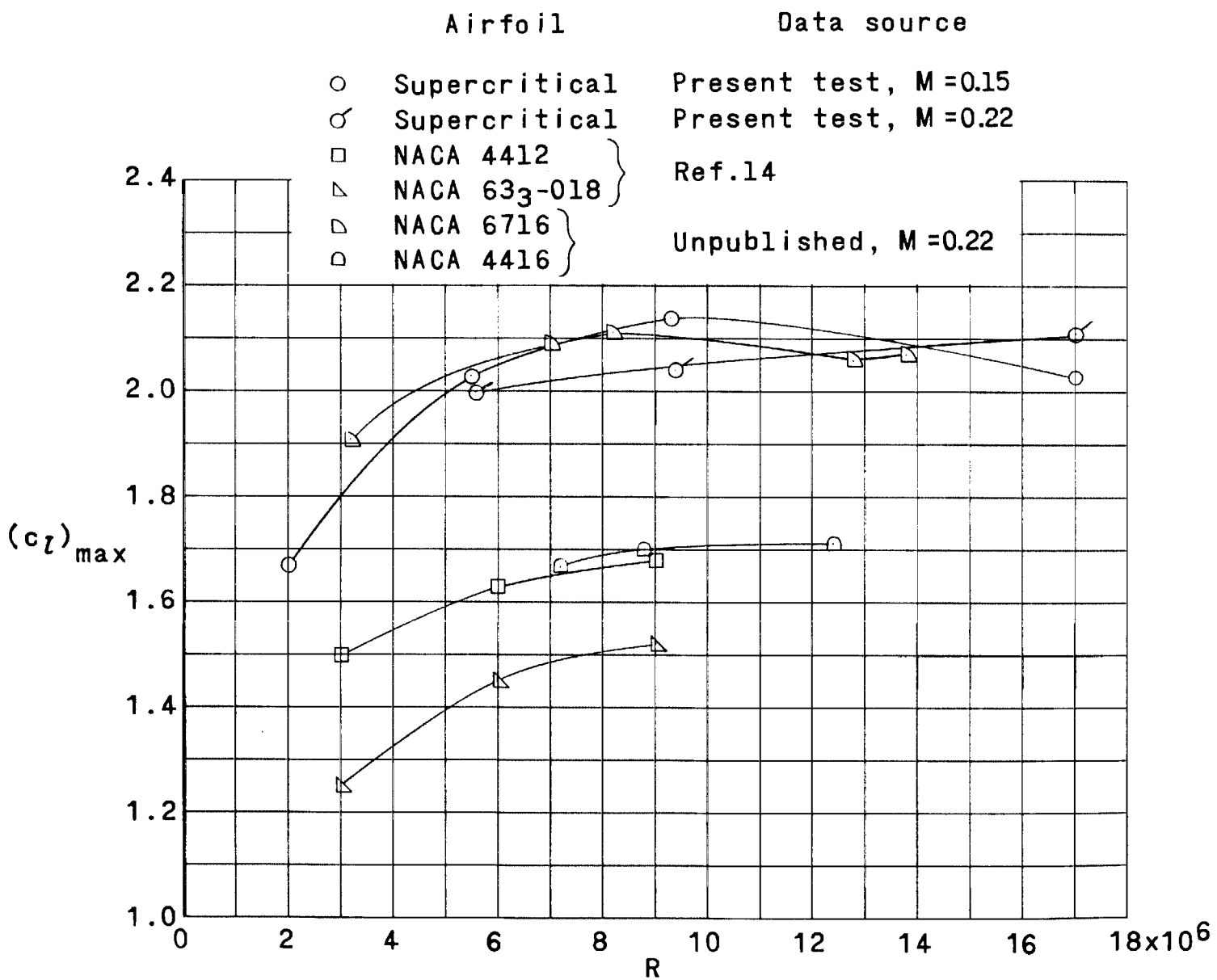

Figure 12.- Variation of maximum section lift coefficient with Reynolds number for various airfoils.

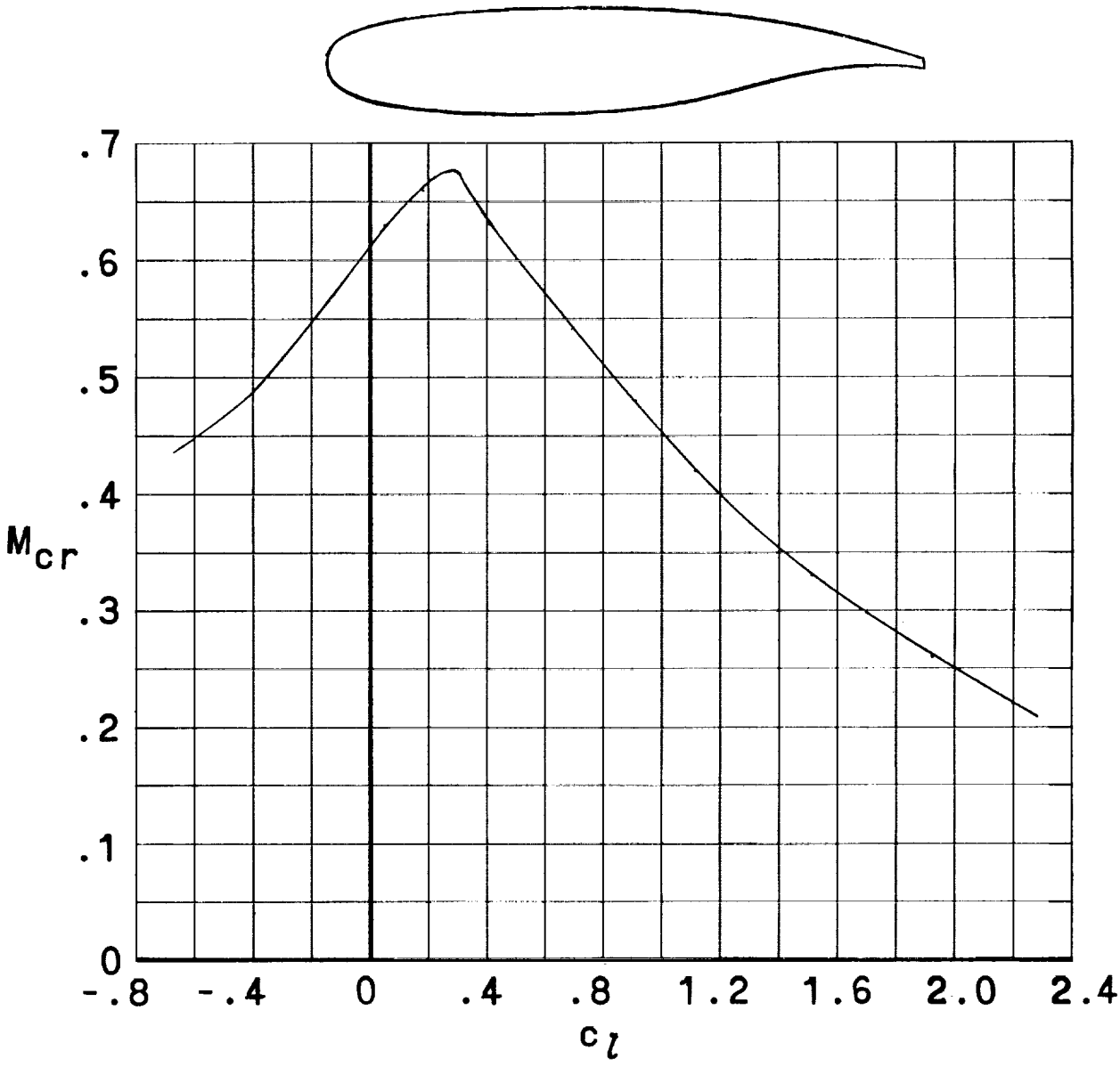

Figure 13.- Variation in critical Mach number with section lift coefficients.

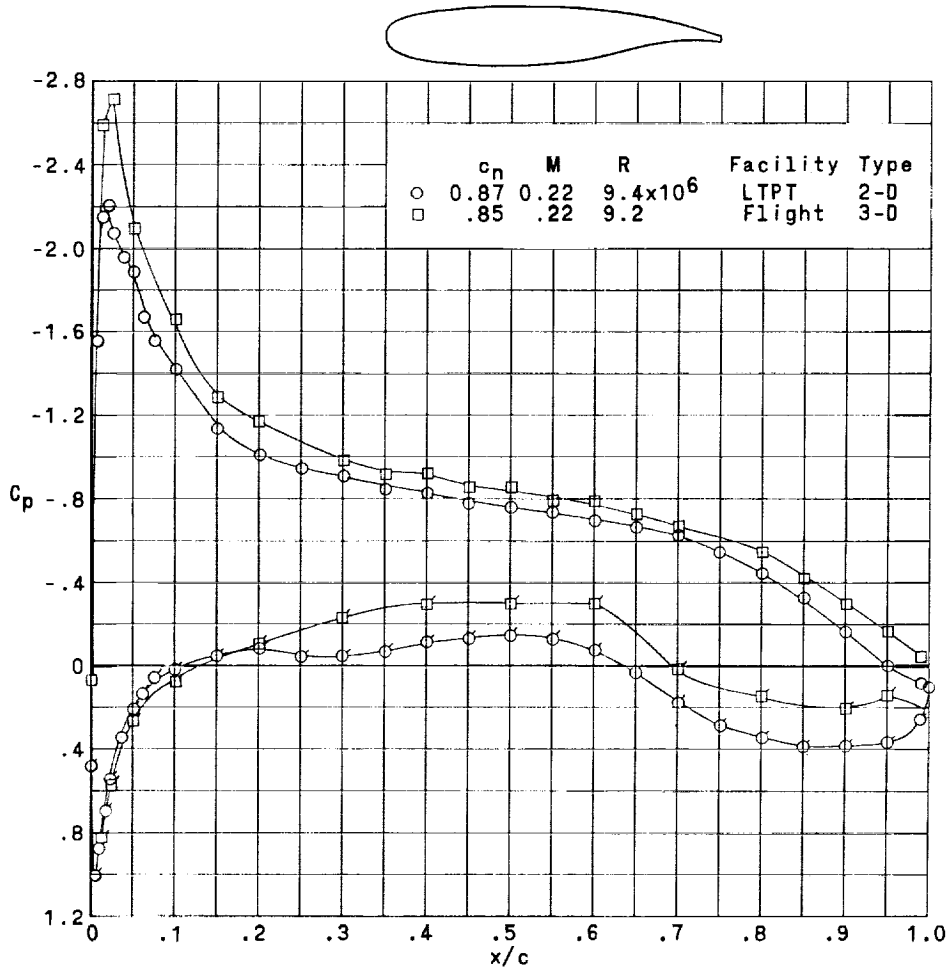

(a) M = 0.22; $c_n \approx 0.85$; $R \approx 9.0 \times 10^6$. (Flagged symbols indicate lower surface.)

Figure 14.- Comparison of wind-tunnel and flight chordwise pressure distributions.

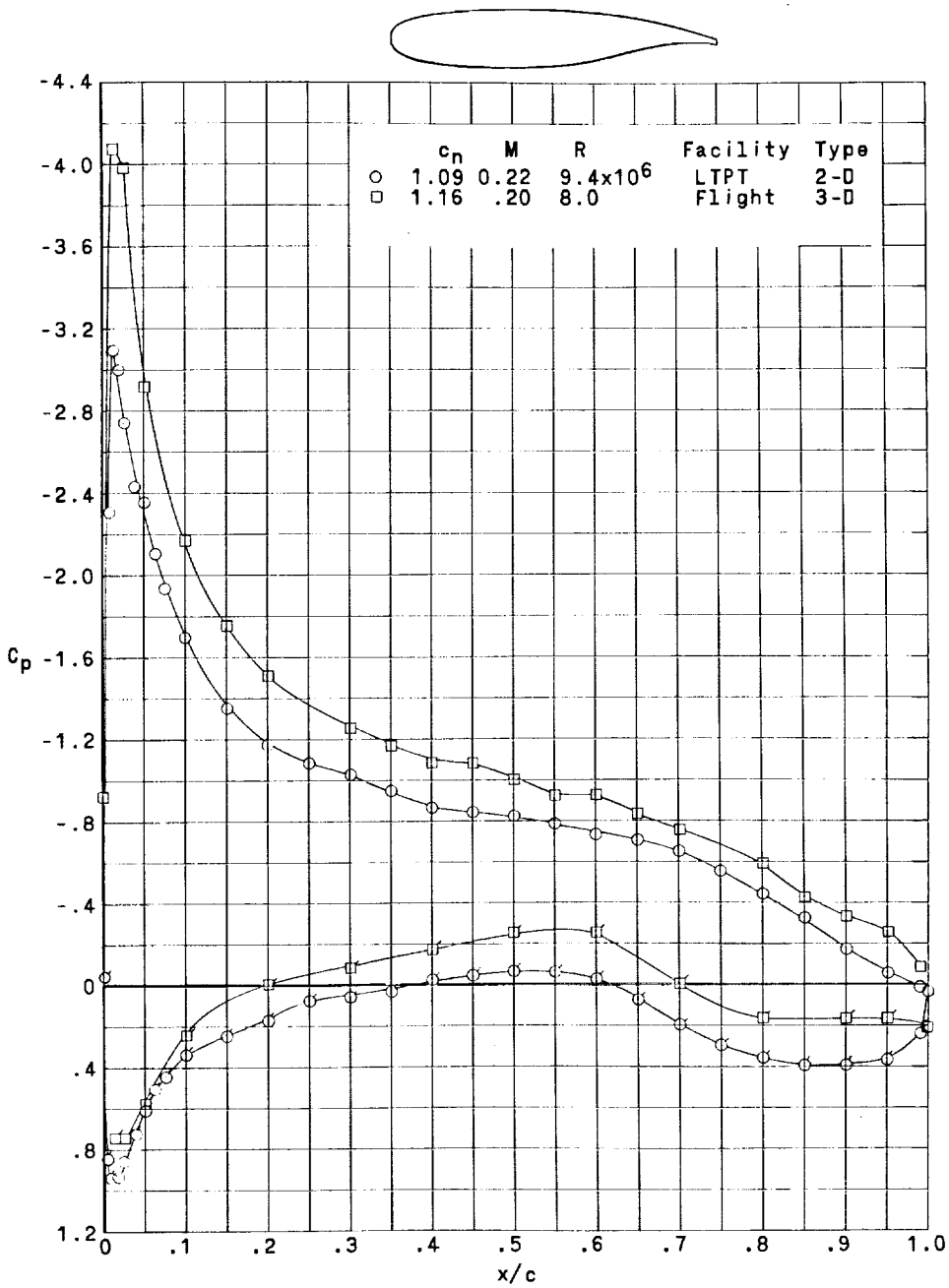

(b) $M \approx 0.20$; $c_n \approx 1.00$; $R \approx 9 \times 10^6$. (Flagged symbols indicate lower surface.)

Figure 14.- Continued.

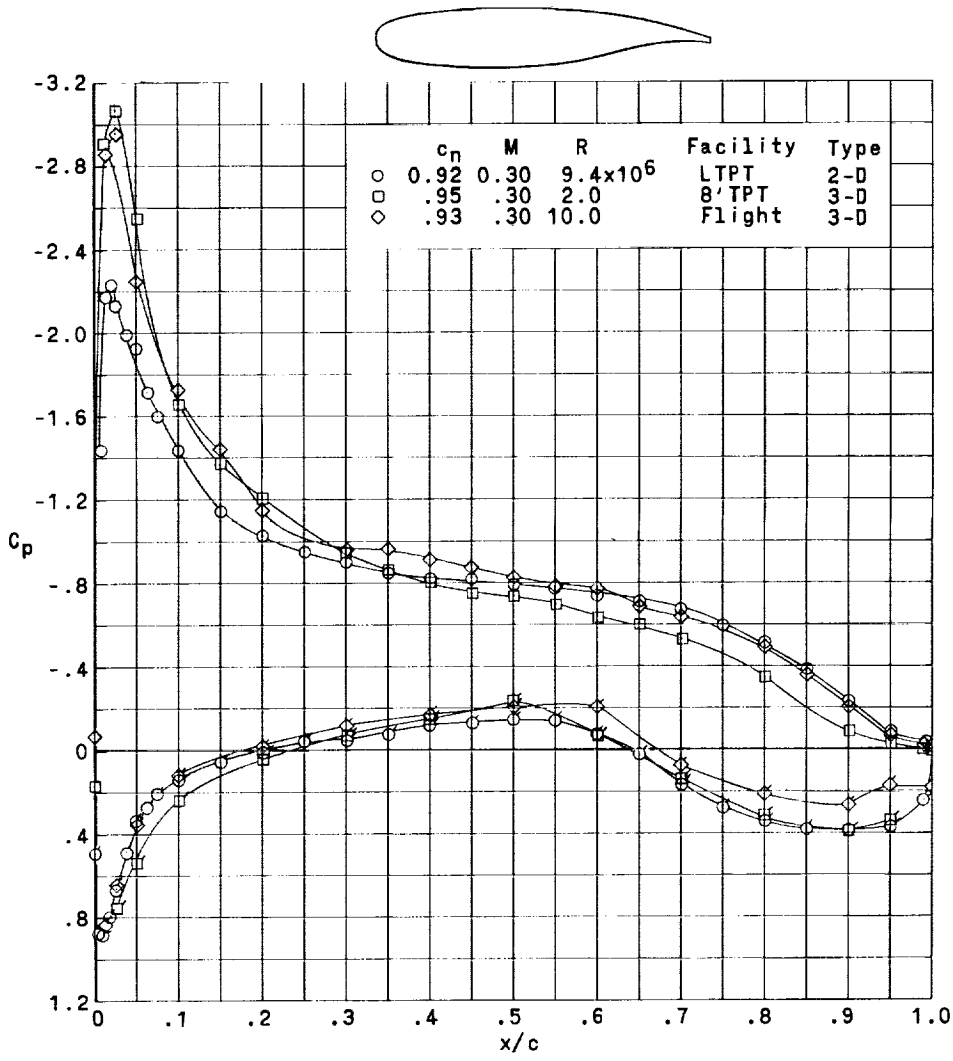

(e) M = 0.30; $c_n \approx 0.90$. (Flagged symbols indicate lower surface.)

Figure 14.- Continued.

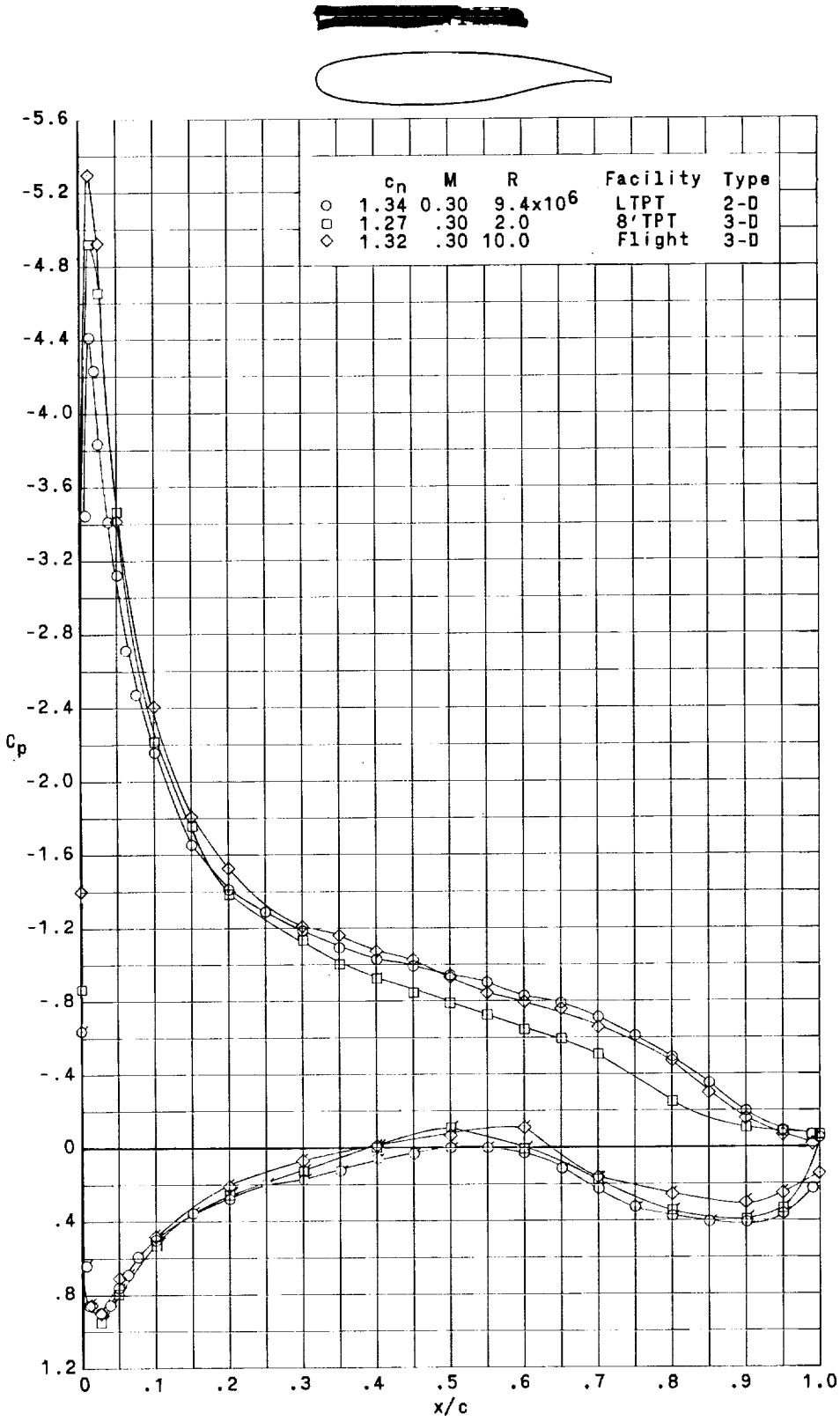

(f) M = 0.30; $c_n \approx 1.30$. (Flagged symbols indicate lower surface.)

Figure 14.- Concluded.

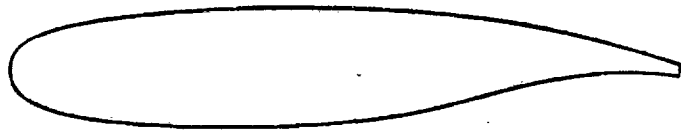

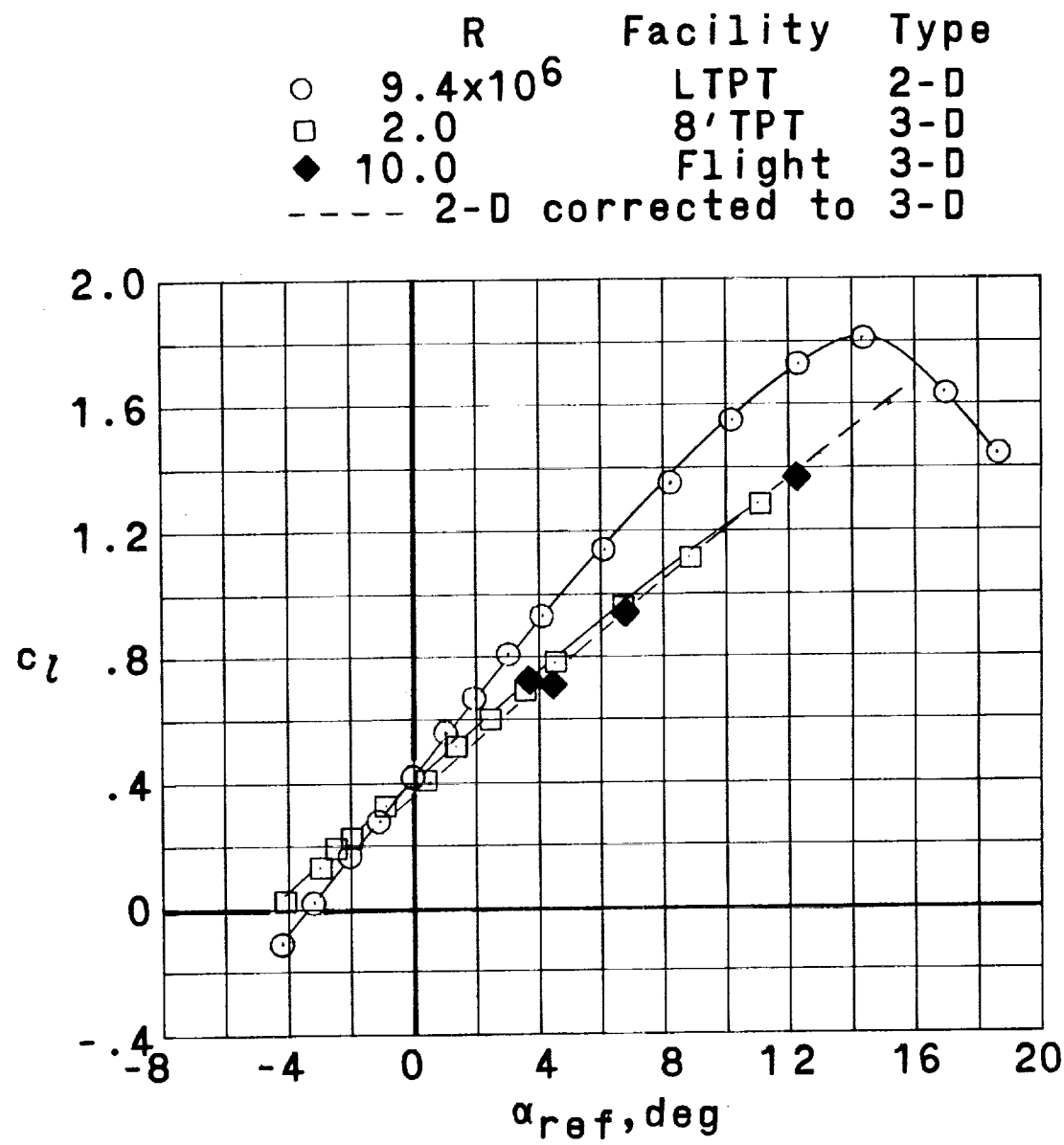

Figure 15.- Comparison of wind-tunnel and flight lift characteristics at M = 0.30.

NASA-Langley, 1972 — 1 L-8290